

**Ball Bonder Rear Y Slide Noise and Vibration Reduction
With Tuned Mass Dampers**

A Thesis
Submitted to the Faculty
of
Drexel University
by
David J. Haruch
in partial fulfillment of the
requirements for the degree
of
Master of Science in Mechanical Engineering

June 2022



© Copyright 2022

David J. Haruch. All Rights Reserved.

Acknowledgments

I would like to primarily thank the employees and managers of the ball bonder group of Kulike and Soffa, Inc. in Ft. Washington PA. Specifically Greg Cutilli, Sean Tracy, Jesse Parish, Eric Myers, and all other members of the BBME team. Without your guidance and support, this project would not have been possible.

While not directly related to this thesis, I would like to thank the members of the Drexel University Formula SAE team. The vast majority of my machining, programming, and design knowledge can be traced back to projects I've worked on for the team. Thank you to Josh Welsh, Nick Bilancio, Amir Daliri, Jon Keller, and Sean Kennedy for being mentors, peers, and an inspiration to achieve more.

Thank you to my advisor, Dr. Dimitrios Fafalis, for being an invaluable aid in writing this thesis.

Thank you to Lauren for all her support.

Lastly, I would like to thank my parents, Joanne and David. Thank you for supporting me in every way imaginable so that I could pursue my goals. I hope that I have made you proud.

Table of Contents

List of Tables	v
List of Figures	vi
Abstract	ix
1 Background	1
1.1 Ball Bonder Machine Background	1
1.2 Competitor Analysis/Use of TMD in the Industry	3
2 Literature Review	6
3 Experimental Modal Testing	8
3.1 Tap Testing	8
3.2 Linear Motor Excitation Testing (“Bode Modal”)	10
3.3 Position Sensitivity	11
3.4 Acoustic Testing	13
4 Rear Y Slide Finite Element Model	17
4.1 FEA Without Bearings	17
4.2 Complication of Roller Bearings	19
4.3 Stiffness of Roller Bearings	20
4.4 Simplified Method To Include Roller Bearings In Modal FEA	21
4.4.1 Comparison of FEA Results to Experimental Modal Data	23
4.5 FE Model Mass Fractions as They Apply to TMDs	27
5 Parameter Optimization of a Tuned Mass Damper	28
5.1 Equations of Motion, Derivation of Cost Functions	29

5.2	Frequency Uncertainty for Robust Performance	31
5.3	Design Curves for Common Mass Ratios	33
6	Design, Prototyping, and Testing of Tuned Mass Dampers	36
6.1	Spring Element Design	36
6.2	Mass Element Design	37
6.3	Damping Source Design	38
6.3.1	Fluid/Grease Based Damping	38
6.3.2	Eddy Current Damping	38
6.3.3	Viscoelastic Material Damping	39
6.4	Testing of TMD Designs	43
6.4.1	Design Iteration 1	43
6.4.2	Design Iteration 2	46
7	Future Work and Recommendations	50
7.1	Summary	50
7.2	Future Work	50
List of References		52
A	Investigation of Non-TMD Noise/Vibration Control Solutions	57
A.1	Addition of Damping/Acoustic Material	57
A.2	Increasing Stiffness by Bonding Components	58
B	MATLAB Code for TMD Parameter Optimization	60

List of Tables

1	Material properties for Rear Y slide extrusion only FEA	17
2	Correlation summary between rear Y extrusion FEA and experimental tap testing	18
3	Material properties for Rear Y slide FE model	23
4	CBUSH spring properties for Rear Y slide FE model	23
5	Correlation summary between rear Y with bearings FE model and experimental tap testing	27
6	Rear Y Slide FE Model Mass Fraction Table	28
7	Optimal damping ratio fit parameters	35
8	Optimal frequency ratio fit parameters	35
9	Candidate materials list for tuned mass	37
10	Material properties for evaluation of a flexure based free layer damping design	43
11	Example computed loss factors for evaluation of a flexure based free layer damping design. Values in bold indicate viable design parameter combinations within adjustment range for an optimal TMD design	43
12	Results summary of on-bonder TMD testing	49

List of Figures

1	(a) Kulicke and Soffa “Rapid Pro” automatic wire bonder (b) SEM image of wire bonded connections on a device	2
2	Photograph of the XY table assembly	2
3	Photograph of the Rear Y Slide assembly disconnected from the X axis	3
4	Photograph of “competitor S” Y axis tuned mass damper	4
5	Photograph of “competitor S” Y axis tuned mass damper laminated shim stack	5
6	Photograph of “competitor A” optics tuned mass damper	6
7	Tap testing results of the Rear Y Slide assembly as mounted on its bearing assembly	10
8	Representative block diagram of the X and Y axis control systems, noise injection locations indicated in red	11
9	Example of “Bode-modal” test data output (red: y axis, green: x axis, blue: z axis)	12
10	“Bode-modal” vibration testing at 7 XY table positions	13
11	(a) Free extrusion acoustic tap testing setup (b) accelerometer FRF (red) microphone FRF (blue)	14
12	“Bode-modal” audio test setup (a) accelerometer location #7 (b) microphone and accelerometer location #11	15
13	Photographs of XY table acoustic tap testing setup	16
14	Tap testing 21 points of FRF magnitude data (a) microphone only (b) microphone (red, Pa/g) and Z accelerometer (blue, g/g)	16
15	Modal FEA Results of free extrusion only. (a) first bending mode. (b) first torsion mode. (c) torsion + bending mode.	18
16	Free hanging modal tap testing results for the first 3 modes of a rear Y slide extrusion	18

17	CAD models of the Rear Y Slide assembly	19
18	Example bearing stiffness data supplied by bearing manufacturers [21] . . .	20
19	(a) Rear Y slide FE model with CBUSH spring elements included. (b) inset view of CBUSH elements colored in red	22
20	Rear Y with bearings FE model Mode 1: “Y rigid body”	24
21	Rear Y with bearings FE model Mode 2: “Overhang bending”	25
22	Rear Y with bearings FE model Mode 3: “Overhang + FY bending”	25
23	Rear Y with bearings FE model Mode 4: “X Flexing”	25
24	Rear Y with bearings FE model Mode 5: “Overhang Bending + Twisting” .	25
25	Rear Y with bearings FE model Mode 6: “MW + Extrusion 1st bending” (sectioned view)	26
26	Rear Y with bearings FE model Mode 7	26
27	Rear Y with bearings FE model Mode 8: “MW + Extrusion 2nd bending (sectioned view)”	26
28	Simplified tuned mass damper diagram	29
29	Response surface generated by parameter optimization MATLAB script .	34
30	Peak optimal damping ratio curves for different mass ratios	35
31	Peak optimal frequency ratio curves for different mass ratios	36
32	Normalized performance curves for different mass ratios	37
33	Soundcoat DYAD 601 damping material nomogram	39
34	EAR SL20300 damping material nomogram	40
35	Free layer damping design parameter diagram	41
36	Design chart for free layer damping	42
37	Initial TMD protoype, note bending of clamping mechanism	44

38	TMD revision 1 natural frequencies (a) first bending mode 1843Hz (b) second twisting mode 4602Hz	44
39	Tap testing FRF data of first TMD design (a) Low bolt tightening torque (b) High bolt tightening torque	45
40	3 bolt TMD design (a) FRF magnitude data with varying cantilever length (b) Photograph of tap test setup	45
41	Second TMD design FEA results (a) Mode 1 1897Hz (b) Mode 2 2890Hz .	46
42	Photographs of the second TMD design revision setup for laser vibrometer and accelerometer testing	47
43	Second TMD design tap testing (a) FRF Magnitude results, (green: no TMD, coral: .060in layer EAR SL, blue: .120in layer EAR SL) (b) Photograph of test setup	47
44	On bonder TMD testing setup photos	48
45	Measured vibration Bode plots with various TMD setups. Right view inset 1700-2100Hz (Black: No TMD, Orange: Un-damped TMD, Purple: TMD with .060in of EAR SL material, Green: TMD with .120in of EAR SL) .	49
46	Commercially available damping material adhered to Rear Y	57
47	Tap testing results of a Rear Y slide with damping material (orange) compared to a baseline Rear Y Slide (navy blue)	58
48	Photo of epoxy bonding layer between Rear Y Slide extrusion and magnetway	59
49	Tap testing results of a Rear Y slide with epoxy bonding (green) compared to a baseline Rear Y Slide (navy blue)	59

Abstract

Ball Bonder Rear Y Slide Noise and Vibration Reduction With Tuned Mass Dampers

David J. Haruch

Dr. Dimitrios Fafalis

As technology advances, demand for higher speed, higher precision machine tools and assembly equipment drives research to meet this demand. Ball bonder machines create small wire bonds between a silicon die and an assembly package by moving a set of automatic bonding tools along a programmed path as fast as possible to create a complete semiconductor device. Recent industry trends have shown demand to reduce noise and vibration during XY motion table movement. Some existing methods to reduce noise and vibration in XY table systems have significant cost or moving mass implications, which can be undesirable for the moving masses in a high speed ball bonder machine.

A tuned mass damper (TMD) is proposed as a solution method to reduce noise and vibration of a certain ball bonder machine XY table component. The relevant portions of the machine were characterized with experimental modal testing and finite element models. Satisfactory agreement was found between FEA and modal/acoustic testing. Optimal design parameters and their sensitivities for the proposed tuned mass dampers were investigated in simulation. Optimal parameters for a robust mass damper design were found to differ from traditional optimal design parameters. Multiple iterations of prototype TMDs were conceptualized and fabricated to fit within packaging constraints, material limitations, and environmental factors. The performance of these prototypes were tested on a complete ball bonder machine. The prototypes showed satisfactory performance to the target mode, but did not show broadband noise or vibration reduction.

1 Background

1.1 Ball Bonder Machine Background

Kulicke and Soffa (K&S) is a leading provider of semiconductor packaging and electronic assembly solutions supporting the global automotive, consumer, communications, computing, and industrial segments. One large part of the business supports research and development of industry leading automatic wire bonding machines.

Wire or ball bonding is a cost effective semiconductor package assembly process. Thin ($18\text{-}50\mu\text{m}$) gold, silver, or copper wire is bonded to connect bond pads on a silicon die and assembly package pad with a combination of heat, pressure, and ultrasonic vibration. A K&S bonder and an image of a bonded device are shown in Figure 1.

To move the bondhead to different locations on the device to be bonded, an XYZ motion table is used. A system of linear motors, precision bearings, flexures, encoders, and complex control systems are used to guide this motion. To bond devices as quickly as possible, the XYZ motion table must be extremely fast (large acceleration/jerk) and extremely precise. Precision on the order of $3\mu\text{m}$ (3σ) and XY table acceleration of $15+\text{g}$ are common in the industry.

Recent trends in the industry have resulted in a research and development push to reduce audible noise and vibration of the XY table assembly during operation. The requirements of fast and precise motion conflict with the desire to reduce noise and vibration.

For this work, a specific part of the XY table was selected. The Rear Y Slide consists of an aluminum extrusion, steel magnetway with neodymium magnets bonded to it, and a set of linear needle roller bearing rails to allow relative movement of the assembly. A linear servo motor allows the Y axis position to be precisely controlled. The Rear Y Slide is

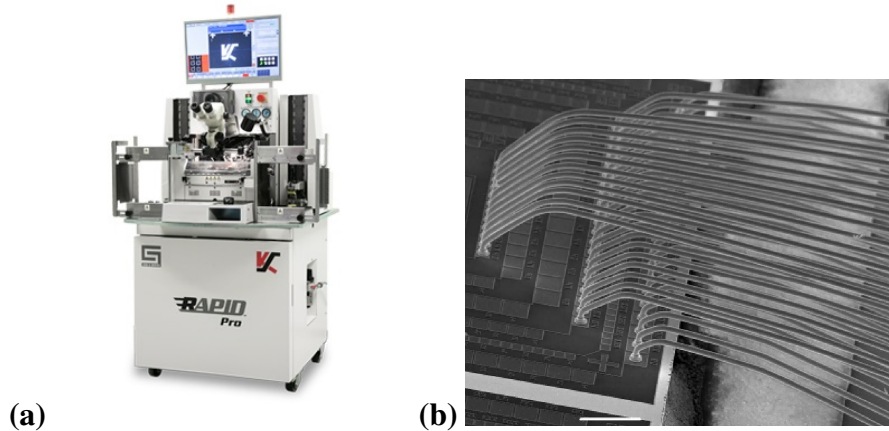


Figure 1: (a) Kulicke and Soffa “Rapid Pro” automatic wire bonder (b) SEM image of wire bonded connections on a device

connected along the Y axis only to the rest of the moving masses of the XY table by a coupling linear bearing and rail combination. A photo of the complete XYZ motion table assembly is shown in Figure 2. A photo of the rear Y slide assembly alone is shown in Figure 3.

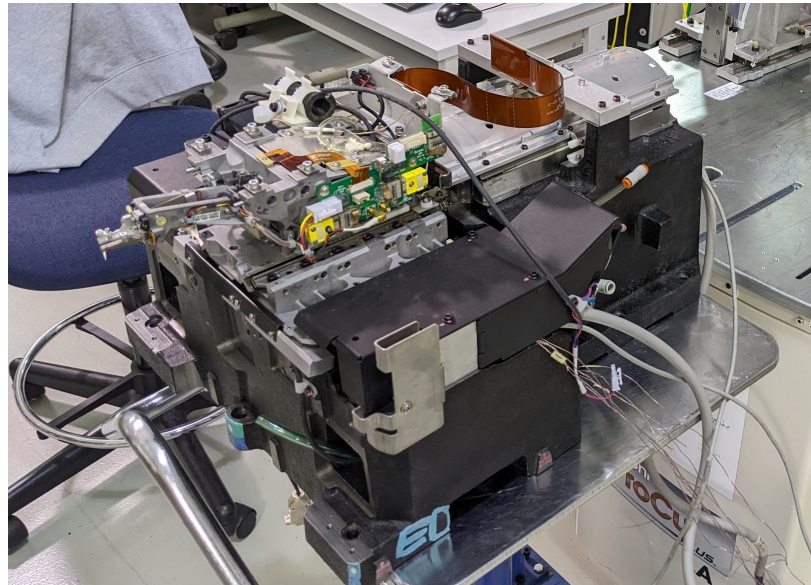


Figure 2: Photograph of the XY table assembly

While there are a wide range of possible solutions to noise and vibration issues, it was chosen to investigate a Rear Y Slide tuned mass damper (TMD) as a solution to

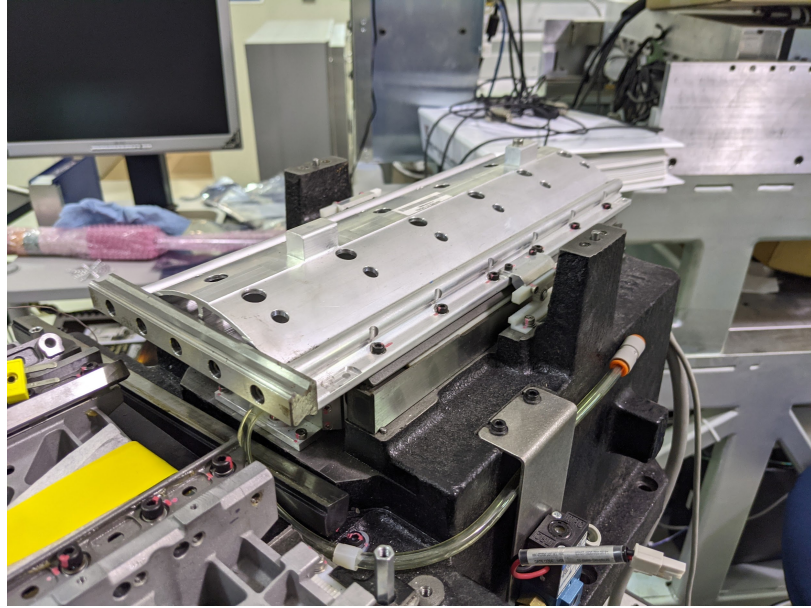


Figure 3: Photograph of the Rear Y Slide assembly disconnected from the X axis

supplement other noise and vibration development efforts at K&S. A tuned mass damper can be most basically described as a mass attached to a vibrating component with a tuned spring rate and damping ratio such that vibration at a natural frequency of the component is reduced.

1.2 Competitor Analysis/Use of TMD in the Industry

Tuned mass dampers have seen use in the ball bonder industry, and the greater semiconductor industry in recent years. Understanding the prior art of commercially successful TMD solutions will give insight into the TMD design process.

Recent developments at Kulike and Soffa have seen tuned mass dampers being used on the transducer component, which produces ultrasonic motion powered by piezo crystals for ultrasonic welding purposes in the ball bonding process. Transducers are designed with certain excitation frequencies in mind, and any parasitic modes from the transducer mounting structure (Z axis link) can interfere with this functionality. Z link natural

frequencies in the ultrasonic range are often difficult to predict reliably even when using high specific stiffness materials like CFRP and beryllium alloys due to manufacturing tolerance and different installed mounting conditions. Using a tuned mass damper, the impact unwanted ultrasonic vibration modes cause can be mitigated [1].

A competitor Y axis design features a patented dual stator, moving coil Y axis motor design [2]. The long cantilevered moving coil necessitated by this design presumably causes issues primarily with the first bending mode of the cantilevered beam Y axis moving coil. To combat this, in their design a high modulus material (CFRP) in a mass efficient structure (foam/honeycomb core panel) is used within packaging constraints to maximize the natural frequency of this mode. To provide damping to the first bending mode of the structure, a tuned mass damper is attached at the end of the beam, shown in Figure 4.

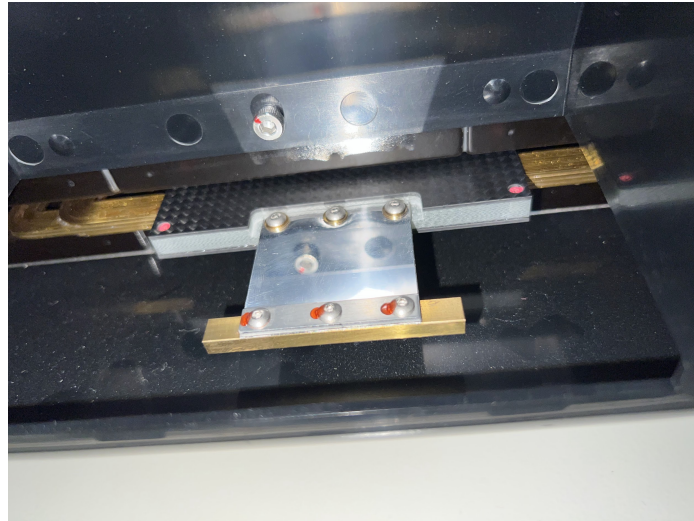


Figure 4: Photograph of “competitor S” Y axis tuned mass damper

No details on the mass ratio, frequency tuning and damping of this device are known. The spring and damping elements are a composite structure of laminated shim steel and a black viscoelastic material. A photograph showing the detailed elements of the tuned mass damper design is shown in Figure 5. The tuned mass is made from a brass like

material. It is assumed that the tuned mass damper increases the Y axis servo performance by damping the first bending mode. Some possible complications to the design could be inherent with the moving coil design and use of viscoelastic materials. A major compromise of moving coil design is that more heat in the coil is generated under operation compared to a moving magnet design. If this heat reaches the tuned mass damper under high levels of Y axis RMS current, the elastomer materials, which are highly sensitive to temperature, might change properties enough to “detune” the tuned mass damper and significantly reduce its effectiveness.

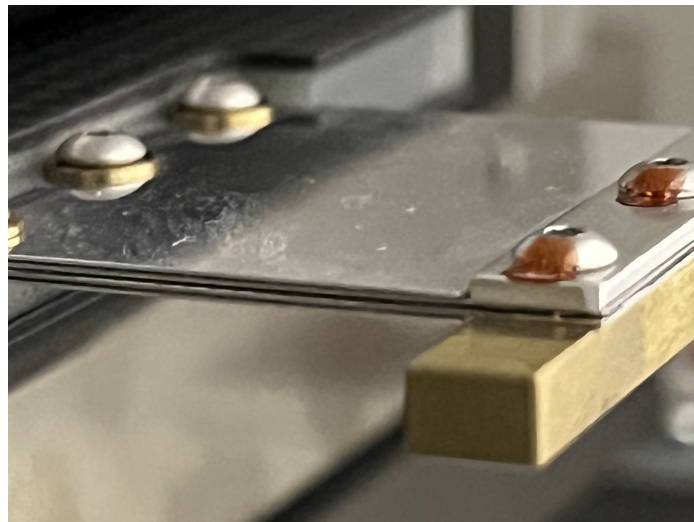


Figure 5: Photograph of “competitor S” Y axis tuned mass damper laminated shim stack

Another competitor optics assembly, which houses a camera and is used to visually align reference marks on the silicon die to the bonder coordinate systems, also features what appears to be a tuned mass damper assembly. Due to process and packaging constraints, the optics assembly is traditionally cantilevered from the main Y axis structure. It is assumed that the tuned mass damper targets the first optics “pitch” mode, which can be one of the lowest natural frequency modes of the entire XY table structure. The tuned mass damper could also target the next highest optics “yaw” mode if it is of a 2DOF design. The tuned mass damper design appears to be a monolithic structure with a flexure integrated into the aluminum or aluminum silicon carbide (AlSiC) MMC casting. A



Figure 6: Photograph of “competitor A” optics tuned mass damper

photograph of the optics assembly is shown in Figure 6, with the black cylindrical assembly assumed to be the TMD device.

2 Literature Review

Tuned mass dampers (TMD) have seen extensive research and development in any industry where vibration can cause issues. This section aims to review the established methods and design process surrounding existing tuned mass damper use.

In the machine tool industry, large, precise holes are typically formed with a boring bar tool in a lathe. The limiting factor on material removal rate and precision especially for very large length to diameter holes, which require a long boring bar cantilever distance, is the mechanical resonance from the first natural frequency of the boring bar. Packaging limitations restrict methods of increasing this natural frequency even if heavy metals or high stiffness materials like tungsten are used. Tuned mass dampers have been used to improve the performance of boring bars [3] and many commercial options [4] are available. Typical designs feature a dense mass packaged within a hole inside the end of

the boring bar. The hole is filled with oil and the bar is suspended on a system of disc springs and o-rings.

Tuned mass dampers have been applied in other tooling for machining in the form of long length to diameter ratio tools [5] or micro-machining tools [6] in a similar way to boring bars.

In general the design process for tuned mass dampers when applied to machine tooling takes similar steps. First, experimental [7] or analytical [8] methods are used to determine a natural frequency of the cutting tool that causes issues with the machining process. For some tools a second or higher natural frequency is also identified to be used in the design of a multi-DOF TMD design. For some applications especially involving high spindle rotation rates, natural frequencies may change significantly across the operating range of the machine tool [9], meaning the TMD design must be robust or targeted at a specific part of the operating range. For some tool designs, the stiffness of the mounting structure of the tool holder may play a significant role in the stiffness of the whole tool assembly [10] [11].

Second, optimal tuned mass damper “tuning” parameters of stiffness and damping are estimated with analytical [12] or computational [13] methods.

Third, a design is fabricated and tuned to the previously found optimal parameters. Test data is compared back to model data to ensure there is a correlation between the simulated optimal parameters and real data.

Tuned mass dampers have been applied in the semiconductor industry outside of wire bonding. Advanced lithography systems require extreme levels of motion precision and control, and as such are suited to application of TMD-based mechanisms [14] [15] [16] [17]. The methods discussed differ slightly from the research in the machine tool industry in that the results of application of tuned mass dampers are discussed from a control system performance perspective, but overall the design process is similar.

3 Experimental Modal Testing

To start the TMD design process and in general understand the nature of the noise and vibration created by the Rear Y Slide, a variety of tests were carried out to experimentally characterize the Rear Y Slide noise and vibration through various methods. This testing aims to identify target mode shapes and natural frequencies that could potentially be damped with a TMD.

3.1 Tap Testing

In modal tap testing, a special impact hammer is used to excite a structure. The force of the impact is recorded in the time domain. Various styles of hammer are available commercially that can alter the energy input into the structure. Various tip types are commercially available to excite the desired range of frequencies. The structures response is measured with various sensors in the time domain. Common sensors are MEMS or crystal based accelerometers, laser doppler vibrometers, or capacitive probe sensors. Transforming both these signals into the frequency domain through a FFT allows a transfer function from force to vibration to be computed. Peaks in this transfer function are the natural frequencies of the part or assembly. The sharpness of these peaks can be used to determine the approximate equivalent viscous damping of each mode.

Multiple types of impact hammer and different tip materials are used throughout this thesis to get satisfactory excitation of different structures. For larger parts, a Kistler Type 9722A500 impact hammer is used. It has a head mass of 100g and a nominal gain of 10mV/N. For smaller parts, a PCB Model 086C01 impact hammer is used. It has a head mass of 100g and a nominal gain of 11.2mV/N. The most commonly used impact hammer tip is a metal tip that allows a measurable frequency range of up to 8000Hz+. Softer

plastic tips and additional mass can be added to the impact hammer to excite different frequencies ranges with different amounts of energy input. Impact hammer use is slightly dependent on the operator skills to provide consistent taps. To mitigate this effect, multiple impacts are used for each measurement point throughout the thesis, and coherence values are checked to confirm the measurement is repeatable.

Two types of accelerometer are used throughout this thesis. First will be referred to as a “triaxial” accelerometer. It is a Brüel & Kjær Type 4520 piezo crystal based accelerometer with a nominal gain of 10mV/G and a weight of 2.9g. This accelerometer is used for measurement of relatively light structures (100g) where the additional mass of the large accelerometer will not influence results and the simultaneous 3 axis measurement will save time when conducting a large scale modal test. Second will be referred to as a “tear drop” accelerometer. It is a Brüel & Kjær Type 4517 piezo crystal based accelerometer with a weight of 0.65g. A Brüel & Kjær Type 2635 Charge Amplifier is used, which has various options for output gain and filtering which are adjusted to suit the nature of the test. This accelerometer is used for measurement of very light structures where the additional setup time and complexity of a laser vibrometer may be undesirable. The natural frequency of all accelerometers is an order of magnitude higher than the frequencies of interest. Unless otherwise noted, a small amount of wax (less than 0.1g) is used to adhere the accelerometers to the part to be measured. This has a very small impact on the mounted natural frequency of the accelerometer[18], but for the frequency ranges of interest and the accelerometers used this is not an issue.

The laser doppler vibrometer used later in the thesis is a Polytec OFV 353 Sensor Head paired to a Polytec OFV 3000 controller. The laser vibrometer will be used whenever the mass and cable of an accelerometer are not suitable for the desired part/setup. Because the laser vibrometer is a noncontacting measurement system, it does not mass-load the part and the only constraint on its setup is line of sight (optionally with mirrors) to the

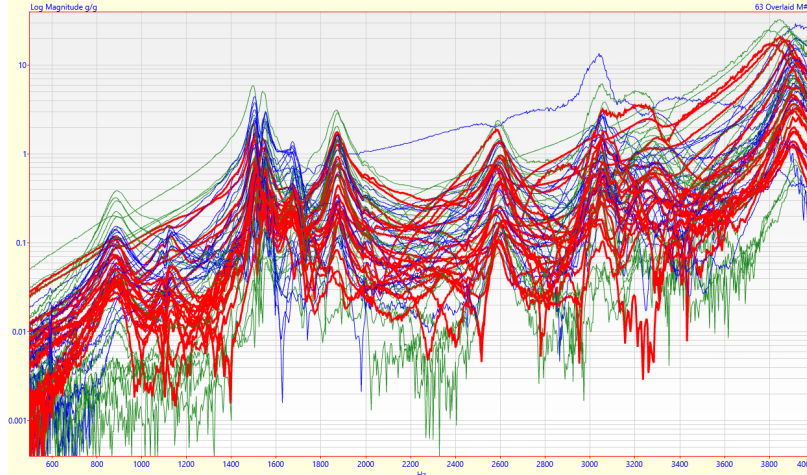


Figure 7: Tap testing results of the Rear Y Slide assembly as mounted on its bearing assembly

measurement point. The internal filtering of the controller is disabled and the velocity gain for most tests is nominally set to 125mm/s/V.

Tap testing was performed on a Rear Y Slide structure both on and off its bearing arrangement. One set of the results of this tap testing at a negative extreme of Y axis travel are shown in Figure 7.

3.2 Linear Motor Excitation Testing (“Bode Modal”)

A representative discrete block diagram of the Y axis controller is shown in Figure 8.

Noise can be injected into various locations in the control loop from an outside source by input pins on the controller board. The noise injection locations are circled in red. For this test procedure, noise is injected into the velocity control loop. All biquad (“BQ”) filters are disabled before the test is run. Feedback gains are set to settings found to work well for this test. Feed forward (Velocity (K_{vff}), Acceleration (K_{aff}), Jerk (K_{jff}), and Snap (K_{sff}) if applicable) gains are tuned with an automatic tuning procedure and confirmed with manual testing of following error over various motion lengths for the specific build of XY table. Because of the fundamental CG height vs Z axis flexure height mismatch, the Z

axis remains enabled during this testing to allow the Y-Z coupling to maintain Z position to avoid any unintended effects of Z axis movement on the Y axis testing.

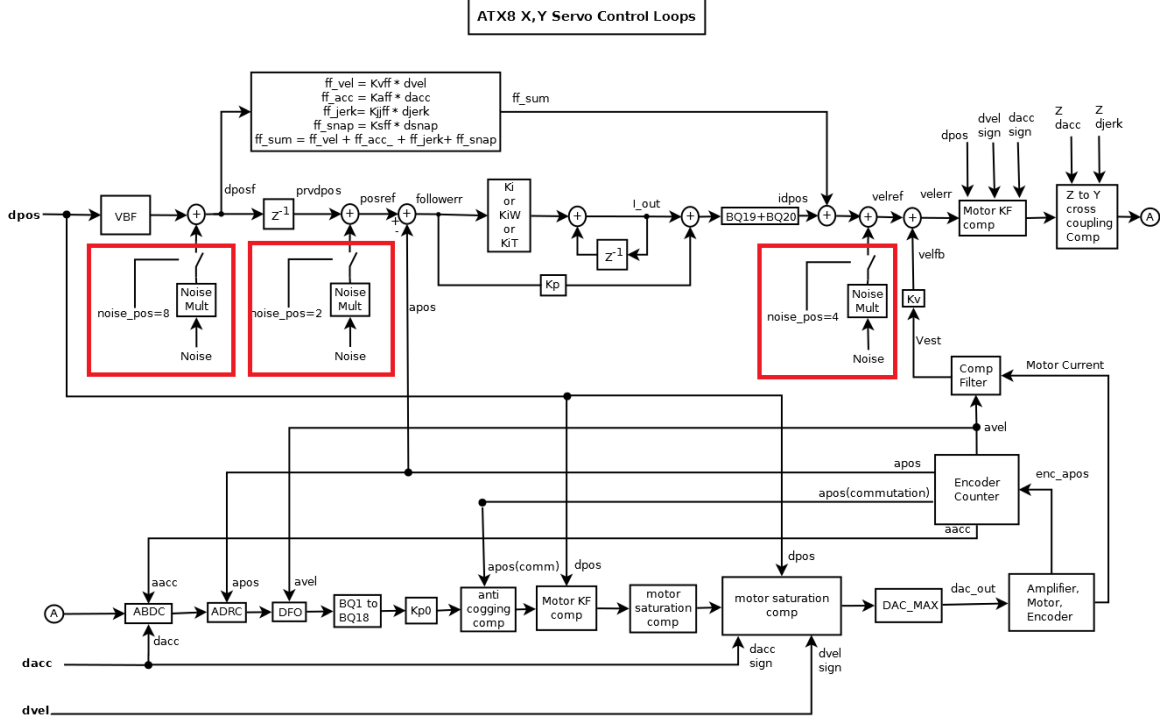


Figure 8: Representative block diagram of the X and Y axis control systems, noise injection locations indicated in red

While any form of noise can be injected into the control loop, typically this test uses either a sine sweep “chirp” or white noise. The input signal is generated by a NI USB-4431 data acquisition device. The desired range and amplitude of excitation from the linear motor can be easily adjusted to suit the test. Noise and vibration outputs can be collected from a “Bode-modal” test.

An example of 21 points of XYZ accelerometer data collected from this test procedure is shown in Figure 9, which shows peaks at 600, 1000, 1500, and 2300Hz.

3.3 Position Sensitivity

“Bode-modal” testing was used to quantify the position sensitivity of the vibration modes

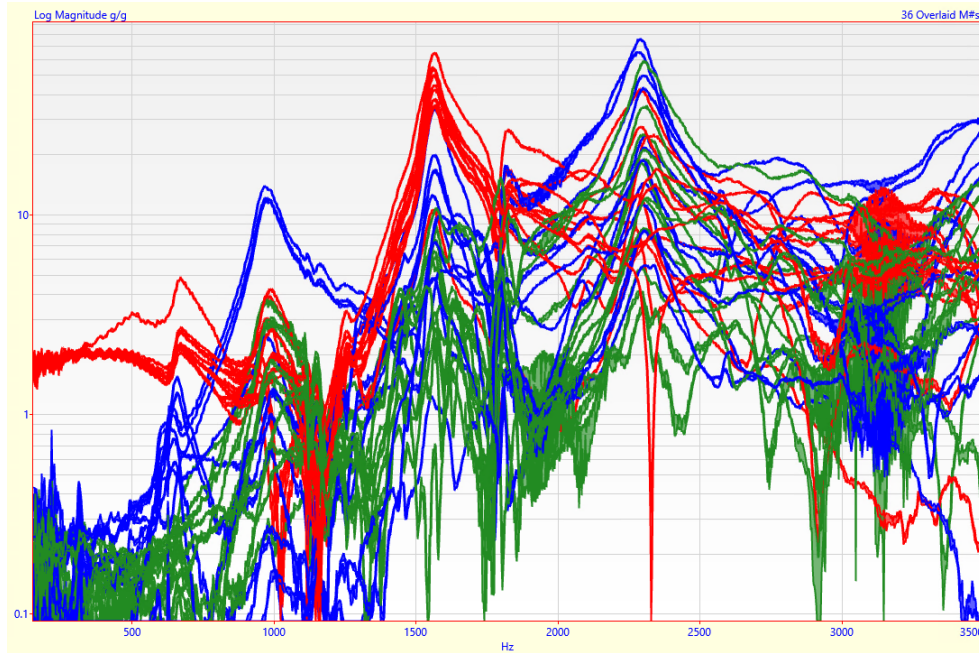


Figure 9: Example of “Bode-modal” test data output (red: y axis, green: x axis, blue: z axis)

of the Y axis. From the bearing support arrangement and CG position of moving masses, the center of machine XY travel will tend to have significantly less vibration than positions on the edges of the machine XY travel. Additionally as the bearing support of the X and Y axes change, mode shapes and natural frequencies can change. The XY table has a rectangular work area with nominally 80mm of both X and Y travel. 7 XY table positions with 21 accelerometer points of XYZ data per position were tested in the table positions indicated in Figure 10 at the extremes of the XY table travel.

In general the results indicate that the table positions at the extremes of X and Y travel will create more vibration as measured at the rear Y slide. This is most likely due to the CG offset of the X axis assembly and change in bearing support at table positions near the end of the travel. Additionally, some modes are table position dependent, while others are not. The sharp peak at 1500Hz, possibly known to be a mode of the Front Y and X axis structure is simply driving a the Rear Y at this frequency, and therefore does not change in frequency with table position. The first natural frequency at 900Hz only appears in the

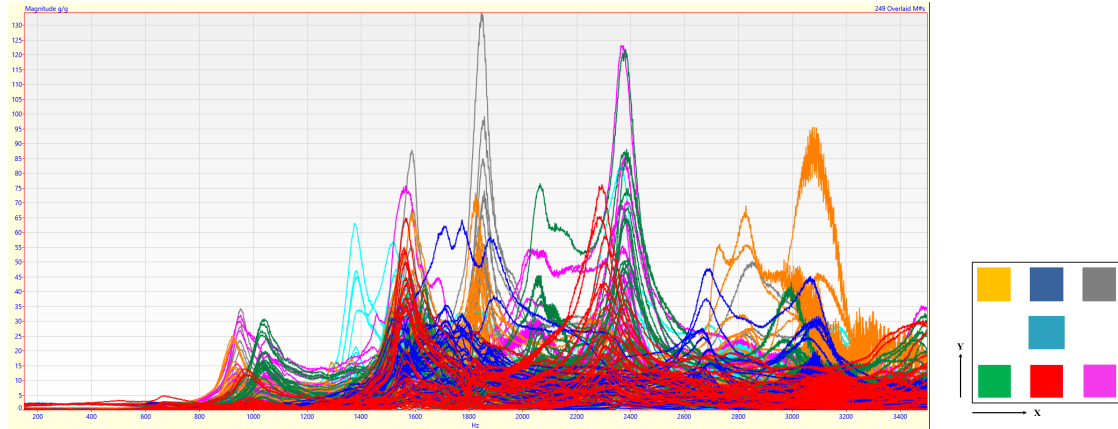


Figure 10: “Bode-modal” vibration testing at 7 XY table positions

rear table positions (-y). The sharpest peaks that range from 1800Hz to 2400Hz change significantly with table position, with +y data being grouped at 1800Hz and the -y data being grouped at 2400Hz.

3.4 Acoustic Testing

To investigate the acoustic impact of vibration, tests with a microphone integrated into the vibration testing procedure were developed. A Brüel & Kjær Type 4189-A-021 microphone with an integrated Type 2671 pre-amplifier was used.

While a general modal tap test will show most normal modes of a structure, it does not indicate which modes will create the most noise. Depending on the distribution of stiffness and mass throughout a structure, some modes will only have a very small part of the structure vibrating, most commonly seen with local bending modes on unsupported or cantilevered regions. It was predicted that these modes would not create significant audible noise compared to modes where the entire structure was vibrating. It was also predicted that a mode that has vibration with significant parts of the structure vibrating that had large normal areas to the direction of vibration would cause the most audible noise.

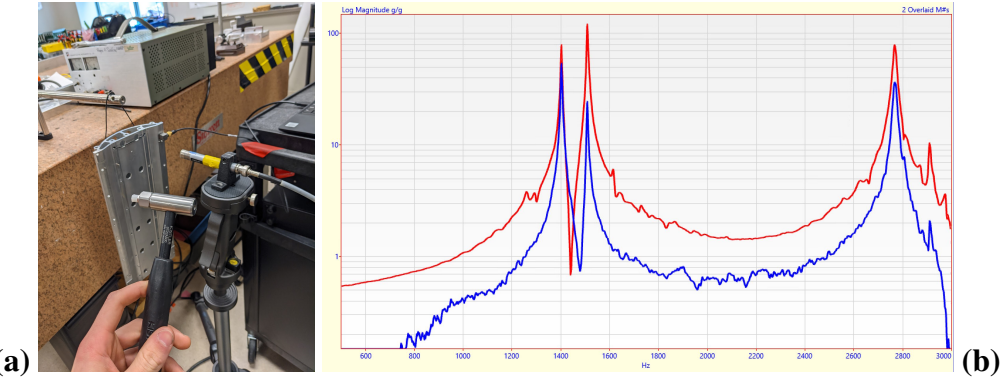


Figure 11: (a) Free extrusion acoustic tap testing setup (b) accelerometer FRF (red) microphone FRF (blue)

To test these concepts, a series of simple tests were carried out. First, a simple case of a free hanging rear Y slide extrusion was first tested to see the correlation between audible noise and vibration. The microphone was placed near the rear Y slide extrusion and the vibration and acoustic transfer functions were computed across multiple runs. Good coherence was found in the measurements, and the vibration modes agreed exactly with the finite element model of the structure. The measured acoustic frequencies were found to match exactly with the measured vibration frequencies, as expected. Also by manipulating the position of the microphone, it was determined that the audible noise emission does depend on the location of the measurement with respect to the operating deflection shape of the vibration mode of interest. A comparison of the acoustic and vibration data and a photograph of the test setup are shown in Figure 11.

Second, a more significantly more complex test was carried out. The “Bode-modal” test setup was modified by removing the X axis output of the triaxial accelerometer, and instead connecting a microphone. Photographs of the test setup are shown in Figure 12. The expected result of this test was something similar to the free hanging extrusion test, but with more noise and inconsistencies in the data due to the additional components. Unfortunately due to the large amount of other vibrating components, surfaces for noise to bounce off, and background noise in the testing lab, no correlation at all was found

between the accelerometer measured vibration and the measured acoustic data. For this reason this test setup was abandoned and a less complex test setup was now needed.

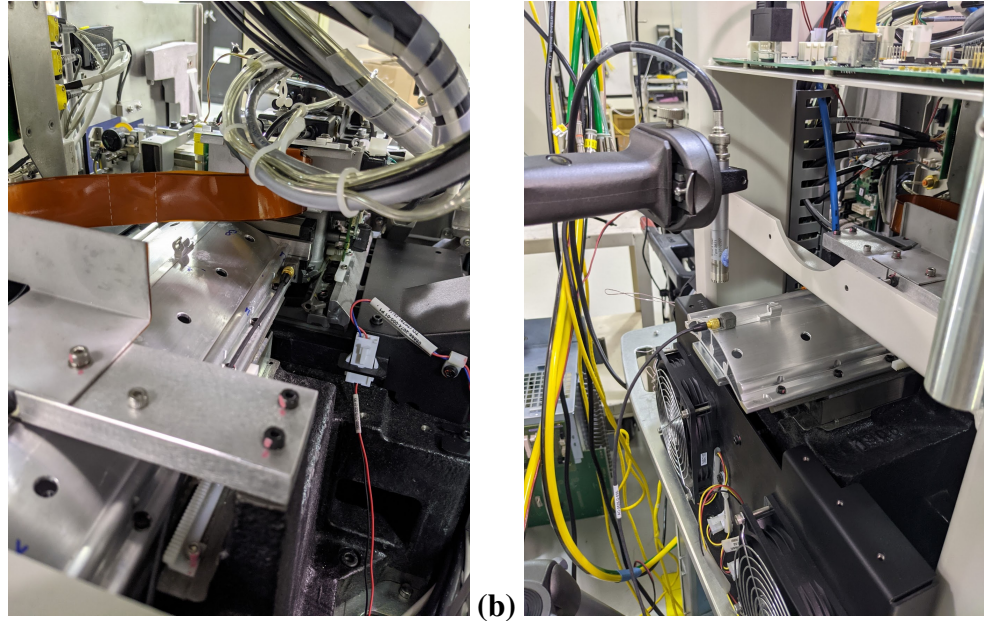


Figure 12: “Bode-modal” audio test setup (a) accelerometer location #7 (b) microphone and accelerometer location #11

Based on the results of the second test, a third less complex test was carried out. The third test was similar to the first, but with a complete assembled XY table used for the tap testing instead of just a rear Y extrusion. Due to the large amount of additional components on the XY table assembly, and vibration modes of the table base casting itself, the results were not as clear. Coherence at critical modes for both accelerometer and acoustic data was quite good above 0.9. The results did confirm the assumptions made about the link between vibration and audible noise. All vibration modes of the rear Y slide showed up as peaks in the audible noise transfer function. However, the modes with the most normal surface area vibrating with respect to the measurement location, showed the most magnitude. Specifically, these are the first and second bending modes of the rear Y slide extrusion. Photographs of the test setup are shown in Figure 13 and a plot of the audio and vibration results are shown in Figure 14. The first and second bending mode peaks of interest are at 1900Hz and 2650Hz.



Figure 13: Photographs of XY table acoustic tap testing setup

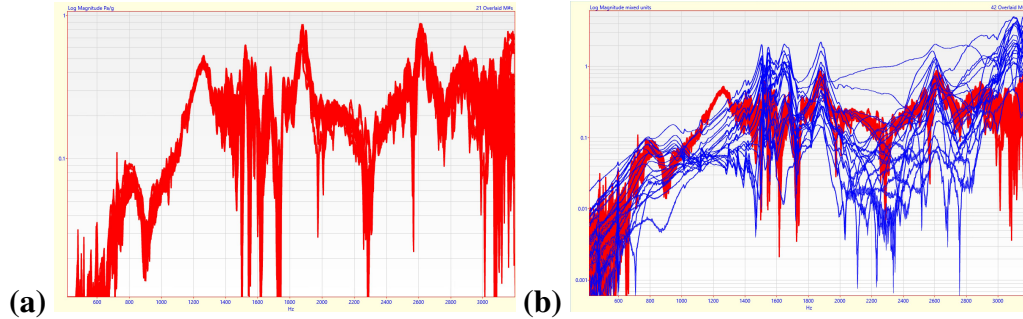


Figure 14: Tap testing 21 points of FRF magnitude data (a) microphone only (b) microphone (red, Pa/g) and Z accelerometer (blue, g/g)

Vibro-acoustic simulation software is commercially available[19], and links between vibration and audible noise have been investigated in the literature[20]. This option was not pursued due to past use of the software having poor correlation with experimental results for another component on the ball bonder machine and the large time investment required to operate the software.

From the results of the combined acoustic, tap testing, and Bode-modal testing, it was decided to consider targeting the 1900Hz and 2600Hz bending modes that showed the highest audible noise and vibration.

4 Rear Y Slide Finite Element Model

Creation of a finite element model of the Rear Y slide was desired to reduce the amount of physical testing needed to understand the vibration modes of the rear Y slide and any possible future design modifications to the parts of the assembly. All FEA in the following sections is done with NX Nastran. All results are from a structural modes solution (SOL103 in Nastran).

4.1 FEA Without Bearings

A simple model was created to ensure the rear Y CAD geometry and material properties were representative of the extruded, machined rear Y slide part. It is difficult to inspect internal and non-machined features of extrusions and past company experience at K&S has seen castings and extrusions deviate slightly from the respective part CAD models. The rear Y slide is extruded from 6063-t6 aluminum. The relevant material properties for a linear modal solution are shown in Table 1.

Table 1: Material properties for Rear Y slide extrusion only FEA

Material	Modulus (GPa)	Poisson's Ratio (ν)	Density (g/cc)
6063-t6 Aluminum	68.95	0.33	2.7

The model was meshed with 4mm second order tetrahedrons for a total of 111702 elements. A quick mesh sensitivity study with a model meshed with 3mm elements showed less than 1% change in all computed natural frequencies so a 4mm mesh was chosen to be a good balance between accuracy and computational cost for future FE models with more components.

The modal solution results of the FEA are shown in figure 15.

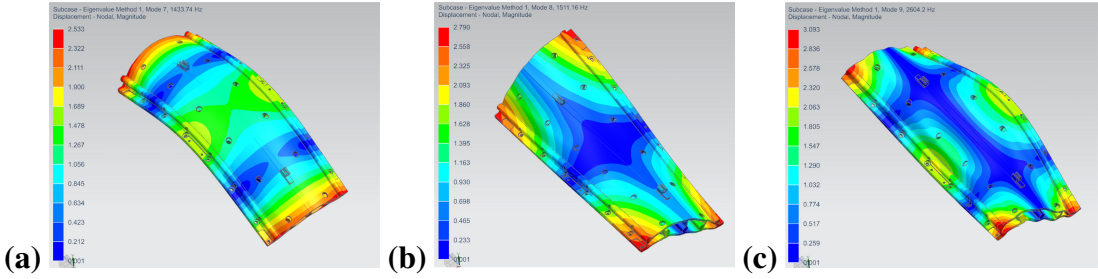


Figure 15: Modal FEA Results of free extrusion only. (a) first bending mode. (b) first torsion mode. (c) torsion + bending mode.

The experimental Bode plot from modal tap testing results is displayed in figure 16.

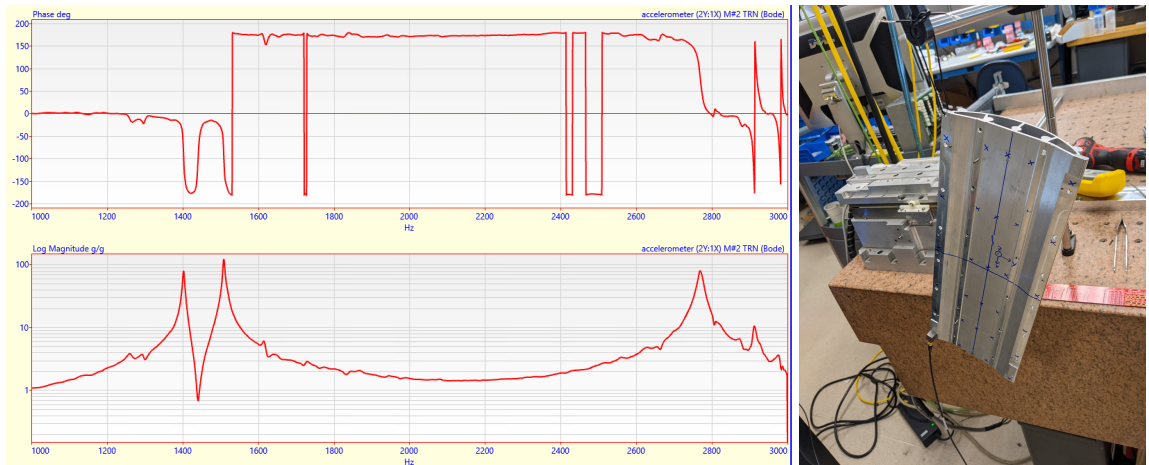


Figure 16: Free hanging modal tap testing results for the first 3 modes of a rear Y slide extrusion

Table 2: Correlation summary between rear Y extrusion FEA and experimental tap testing

Mode	Name	FEA Freq (Hz)	Experiment Freq (Hz)	% error
1	first bending	1434.5	1402	2.3
2	first torsion	1516.9	1508	0.6
3	torsion + bending	2622.1	2768	5.6

These results show that the FEA correlates well with the experimental data.

4.2 Complication of Roller Bearings

A CAD image of the Rear Y Slide bearing arrangement is shown in Figure 17. A photograph of the Rear Y slide bearing arrangement is shown in Figure 3. The arrangement is quasi-kinematic. One side is a “vee” configuration with 2 rows of 1.5mm diameter roller bearings perpendicular to each other. The other side is a “flat” configuration with one row of 2mm diameter roller bearings. While an overconstrained design with two “vee” type rails could give extra stiffness, it is more sensitive to manufacturing tolerance and alignment of the 2 rails. The bearing arrangement is preloaded by the magnetic attraction between the linear motor magnets and stator. Nominally the attractive (preload) force is 500lbf. The Rear Y slide is connected to the rest of the XY table with a linear “coupling” bearing that allows the rear Y to only transmit forces in the Y direction and leaves the rest of the table free to move in the X direction. The addition of these bearings makes FEA of the assembly much more difficult. The stiffness and support offered by the bearings will greatly change the nature of vibration of the Rear Y slide assembly. Therefore, a FE model that incorporates the bearing assemblies was needed.

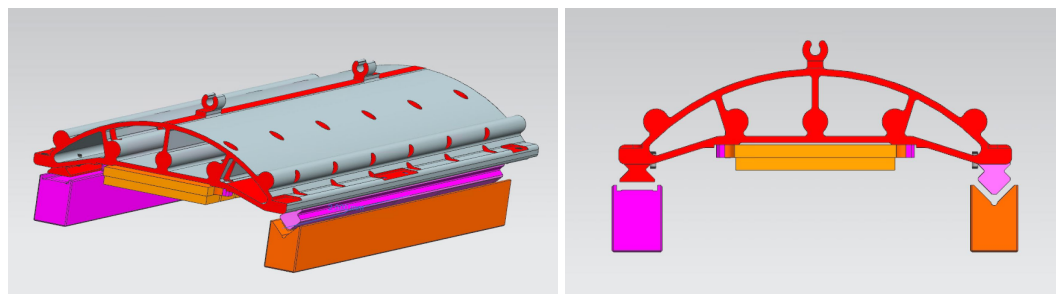


Figure 17: CAD models of the Rear Y Slide assembly

4.3 Stiffness of Roller Bearings

In the design of stiffness based machines and mechanisms, the choice of bearing style and bearing size are critical to meeting stiffness targets for the overall structure. Too small of bearings will not be stiff enough relative to the components they are attached to and may have too short a life to be satisfactory. Too large of bearings will add significant cost and moving mass to the structure.

Bearing suppliers publish stiffness data, but the plots are not tailored to specific applications and represent only common commercially available bearing sizes not used in the specific rear Y slide bearing arrangement. They also do not provide stiffness for off-axis loads or moments. An example stiffness plot from a bearing supplier is shown in Figure 18. For custom applications such as those used on the Rear Y slide, stiffness must be estimated from first principles or empirical testing.

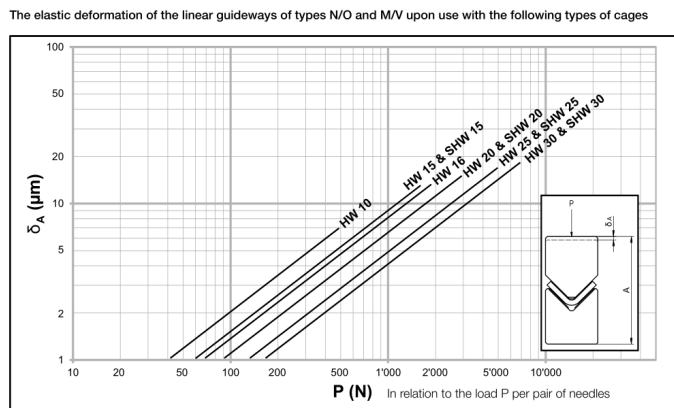


Figure 18: Example bearing stiffness data supplied by bearing manufacturers [21]

Empirical correlations for steel cylinders and steel flats are discussed in [22].

$$\delta = 0.2207L^{-1}P^1D^{-0.3333}[\mu\text{in}]$$

$$\delta = 0.00534L^{-0.765}P^{0.940}D^{-0.053}[10^{-4}\text{in}]$$

$$\delta = 0.00910L^{-0.73}P^{0.6666}D^{-0.080}[10^{-4}\text{in}]$$

A combination of empirical and analytical methods can be used to gather a starting point for the effective bearing stiffness in the FE model.

4.4 Simplified Method To Include Roller Bearings In Modal FEA

The stiffness and placement of bearings on linear axes greatly impacts the natural frequencies and mode shapes of the assembly.

To effectively model bearing contact extremely fine, computationally expensive meshes are needed along with hertzian contact. For common computers, calculation times of multiple hours or even multiple days may be needed for small bearings to get FEA results that correlate well with experimental data. For this reason it was determined that a method of simplifying the rear Y slide bearings in the FEA was necessary, as not including them in the model would show large errors compared to the experimental data.

Methods of simplifying needle bearing contact and stiffness have been investigated in the literature [23][24][25]. Models replacing expensive bearing contact with simplified models in the form of springs and bushings were found to reduce computation time by multiple orders of magnitude while closely matching the stiffness results of a complete FEA with contact analysis. Nonlinear springs to more accurately match hertzian contact were not used again to simplify model complexity.

Due to the geometric arrangement of flat and vee rollers, the spring simplification approach was chosen to model the rear Y slide including bearings. In addition to the cases found in the literature, FEA efforts on other components of the XY table at K&S have shown acceptable agreement with experimental data using the spring simplification method. “CBUSH” elements in Nastran can be used to represent 1D spring/damping elements. Node locations corresponding to the individual needle locations were specified as mesh points in the CAD model to be used during meshing. Each of these matching

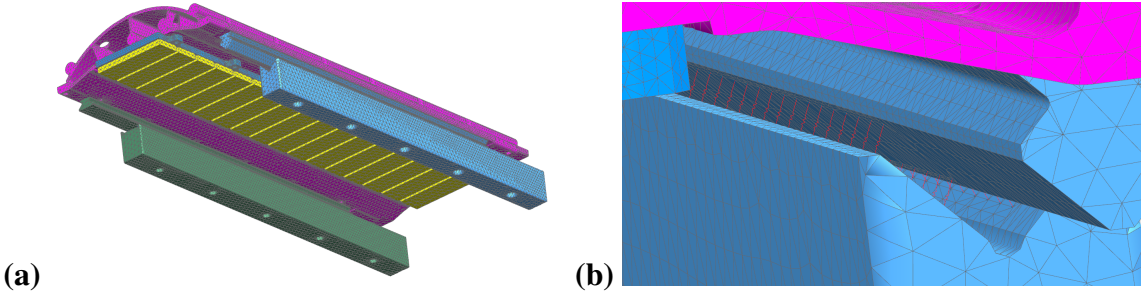


Figure 19: (a) Rear Y slide FE model with CBUSH spring elements included. (b) inset view of CBUSH elements colored in red

mesh point pairs on each bearing race were linked together with a CBUSH element. A meshed model including the CBUSH elements is shown in Figure 19. For modeling simplicity, the connection to the X axis components was not modeled, and testing results discussed previously match this configuration. Future modeling efforts of the complete XY table with close to double or triple the number of bearings and components could be done at the penalty of more complexity and computation time needed.

The flat 2mm and vee 1.5mm rollers were assigned stiffness values. The final stiffness values that were found to agree well with experimental results are shown in Table 4. Because the bearings in the rear Y slide are always under significant magnetic preload, representing bearing clearances by piecewise spring stiffness as found in the literature was not needed. Bearing stiffness is a moderately sensitive parameter that changes the frequency and type of mode shapes. With stiffer bearing values, the soft stiffness of the aluminum extrusion dominates the results. With softer bearing values, the stiffness of the bearings dominates and there is less influence from the aluminum extrusion and steel magnetway on the results.

Connections between components with fasteners was done by the “cone of influence” method from [26][27][28] in order for the computation time of the analysis to remain reasonable. For boundary conditions, Cones of influence on the bottom of the bearing rails were set to zero for all DOF, assuming the table base casting is sufficiently more rigid than

the rear Y slide assembly. Bonded connections were made between magnets and their steel backing as they are bonded with epoxy.

Table 3: Material properties for Rear Y slide FE model

Material	Modulus (GPa)	Poisson's Ratio (ν)	Density (g/cc)
6063-t6 Aluminum	68.95	0.33	2.7
Steel	203	0.3	7.86
Neodymium Magnet	130	0.25	7.0

Table 4: CBUSH spring properties for Rear Y slide FE model

Bearing	Stiffness(mN/mm)	Number of Bearings
flat 2mm needles	13100000	30
“vee” 1.5mm needles	9280000	72

4.4.1 Comparison of FEA Results to Experimental Modal Data

Modal tap testing data was collected with a triaxial accelerometer at 21 accessible points around the Rear Y structure. Satisfactory coherence was found across the structure to show the relevant modes across the frequency range of interest. Data from this tap testing is shown in Figure 7.

Comparisons between the plotted measured mode shapes and the first 8 FEA predicted mode shapes are shown in the below Figures 20 to 27. Not all modes predicted by the FEA were found in the experimental results. This could be due to the excitation location for the tap testing or the limited locations to place an accelerometer or line of sight to point a laser vibrometer at in the assembly. A second possible explanation for the missing modes is that the method of simplifying the needle bearings does not model all aspects of the bearing assembly well leading to modes like the “X Flexing” mode that are not representative of the real vibration modes. This deviation was acceptable as the primary modes of interest around 1900Hz and 2600Hz were well captured. Overall good correlation between the measurements and the FEA was found with a limited amount of

error between the predicted natural frequencies and the measured natural frequencies. One possible source of error is the damping present in the measured modes of roughly 0.2-0.5% critical. Another source of error is the difference in supports from the FEA and the measurements. The table base casting the rear Y slide stationary bearing rails are bolted to is assumed to be rigid in the FEA, however past measurements show that table base casting modes in the 1400-1500Hz range exist that make measurement of the pure rear Y slide modes in the frequency range difficult without a large fixture. A third possible source of error is from the replacement of needle bearings with the spring approximation in the FEA that does not represent the true coupling between the bearing races.

Mode 1 from the finite element solution is not included as it is a rigid body Y axis movement which obviously does not appear in the experimental data. This mode is a consequence of the method used to represent the bearings in the model. The “names” attached to the mode shapes will be used throughout the thesis.

Vibrant Technologies “MEScope” software is used to animate mode shapes from the large number of accelerometer measurements. In the below figures, the left image is the modal FEA solution, and the right image is an animated mode shape from the experimental tap testing data, where the dashed lines are the un-deformed reference state.

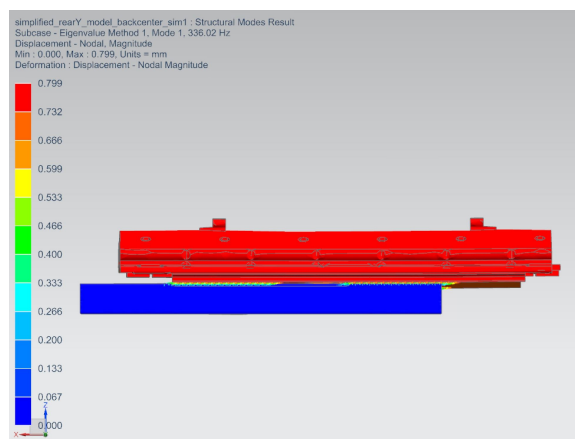


Figure 20: Rear Y with bearings FE model Mode 1: “Y rigid body”

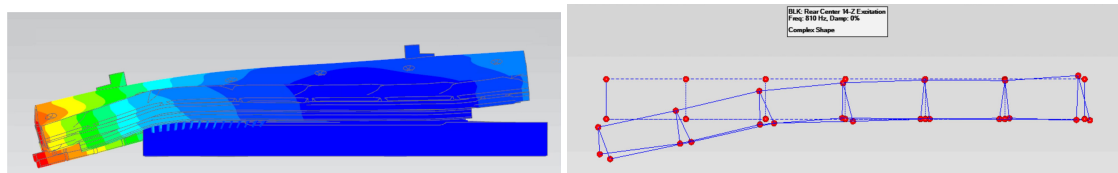


Figure 21: Rear Y with bearings FE model Mode 2: “Overhang bending”

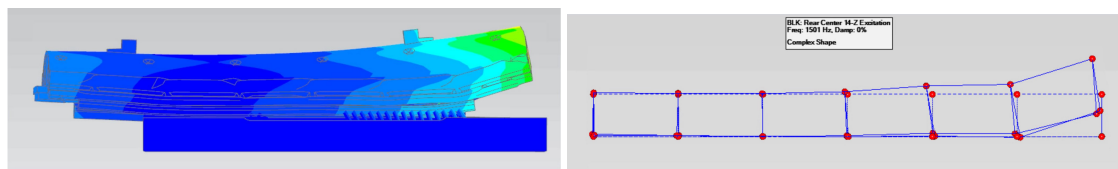


Figure 22: Rear Y with bearings FE model Mode 3: “Overhang + FY bending”

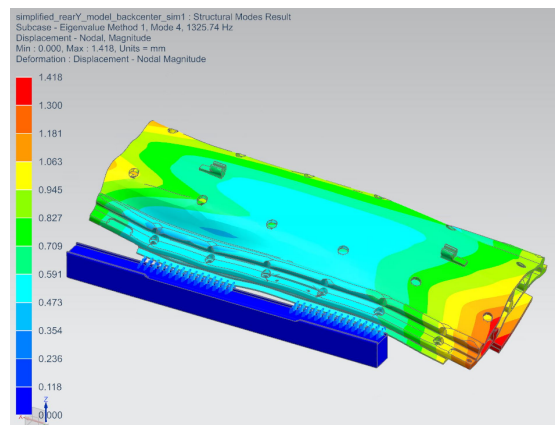


Figure 23: Rear Y with bearings FE model Mode 4: “X Flexing”

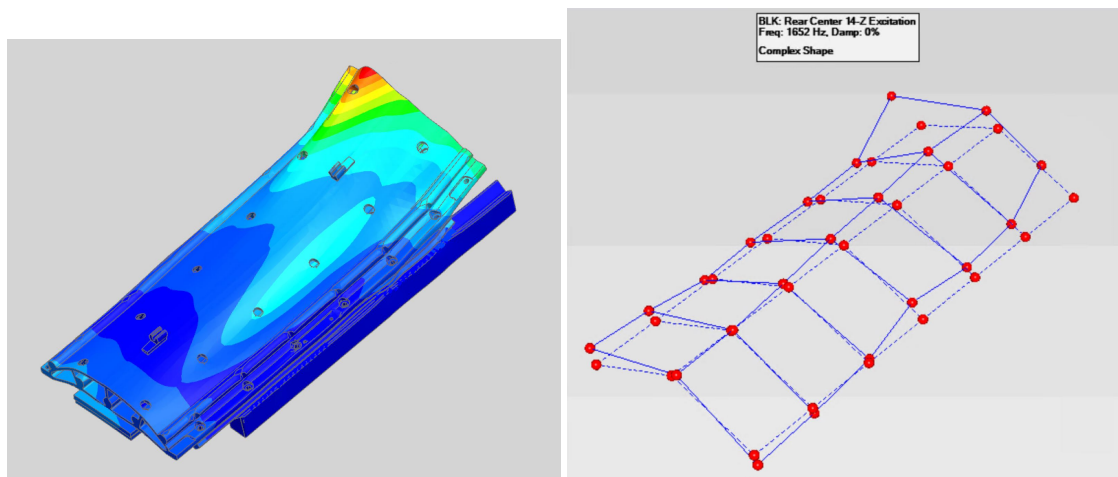


Figure 24: Rear Y with bearings FE model Mode 5: “Overhang Bending + Twisting”

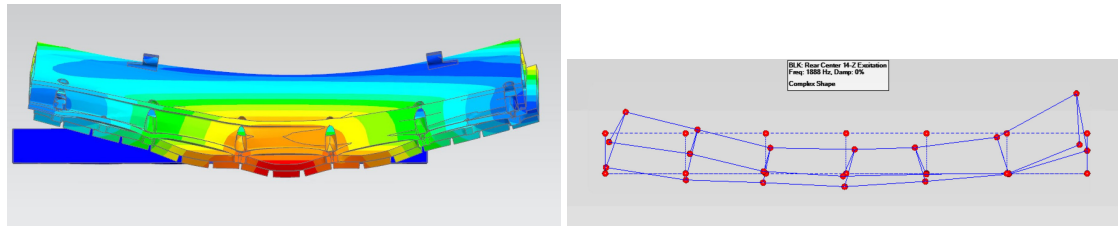


Figure 25: Rear Y with bearings FE model Mode 6: “MW + Extrusion 1st bending” (sectioned view)

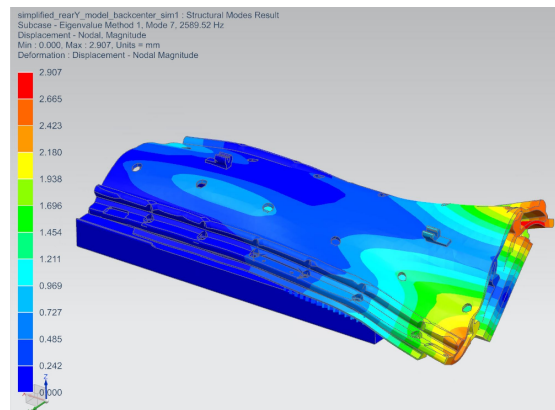


Figure 26: Rear Y with bearings FE model Mode 7

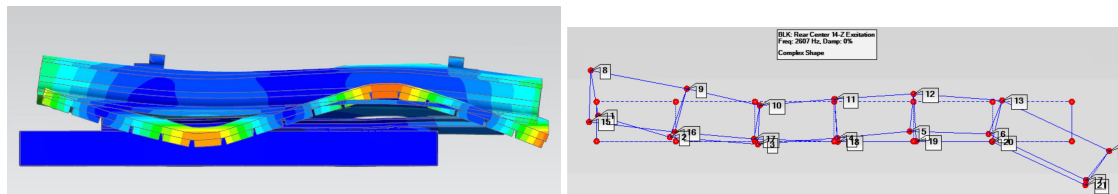


Figure 27: Rear Y with bearings FE model Mode 8: “MW + Extrusion 2nd bending (sectioned view)”

Table 5: Correlation summary between rear Y with bearings FE model and experimental tap testing

Mode	Name	FEA Freq (Hz)	Exp. Freq (Hz)	% error
1	Y Rigid Body	336	N/A	-
2	Overhang Bending	980	792	19.2
3	FY + Overhang Bending	1228	1338	-8.96
4	X Flexing	1326	-	-
5	Overhang Bending + Twisting	1806	1429	20.9
6	MW + Extrusion 1st bending	2002	1927	3.75
7	N/A	2590	-	-
8	MW + Extrusion 2nd bending	2757	2812	-1.99

4.5 FE Model Mass Fractions as They Apply to TMDs

It is desirable to not “over-size” a tuned mass damper by designing a higher mass ratio than is needed to achieve significant vibration reduction. Too high of an effective mass ratio gives diminishing vibration reduction returns as the added mass to the structure quickly increases. Tuned mass dampers above $\mu = 0.2$ are not common if minimizing system mass is a design goal.

In an idealized tuned mass damper model with point masses, computation of mass ratios is simple. However real structures cannot always be approximated as point masses. In a real structure, each vibration mode has a certain percentage of the overall structure mass that engages in the mode. For a simple example, in a cantilevered beam, energy methods can be used to analytically compute the natural frequency and effective mass for the first natural frequency according to closed form equations [29] $f_1 = \frac{1}{2\pi} \left[\frac{3.5156}{L^2} \right] \sqrt{\frac{EI}{\rho}}$ and $\Gamma_1 = 0.7830 \sqrt{(\rho L)}$.

For structures with more complex geometry not able to be simplified, FEA can be used for the same purpose as the closed form equations. Specific flags in NX NASTRAN can be added to output a modal effective mass fraction table. This type of data is difficult to measure without extensive testing and is one of the primary motivations for developing an accurate FE model of the rear Y slide assembly.

The total mass of the components in the rear Y slide FE model is 2955.3g. The Mass participation factor table for the FE model results are shown in Table 6. From these results, tuned mass dampers can be designed where the base system mass can be considered to be the total FE model weight multiplied by the mass participation factor for the DOF and mode the TMD will target. For example, a TMD targeted at the Z DOF of mode 2 would consider an effective base mass of $2955.3g * 0.094 = 277.8g$.

Table 6: Rear Y Slide FE Model Mass Fraction Table

Mode	Freq (Hz)	Description	X Frac	Y Frac	Z Frac
1	336	Y Rigid Body	0.000	0.616	0.000
2	990	Overhang Bending	0.031	0.001	0.094
3	1228	FY + Overhang Bending	0.000	0.001	0.194
4	1326	X Flexing	0.219	0.000	0.000
5	1806	Overhang bending+twisting	0.112	0.000	0.014
6	2002	MW + Extrusion 1st bending	0.074	0.000	0.071
7	2590	N/A	0.045	0.000	0.011
8	2757	MW + Extrusion 2nd bending	0.008	0.000	0.002

5 Parameter Optimization of a Tuned Mass Damper

Optimal parameters for tuned mass damper designs have been extensively studied in the literature. To achieve optimal performance for the Rear Y Slide TMD design, new optimal parameters will be investigated in simulation to ensure the desired tuning parameters are optimal for the Rear Y Slide application.

For simple, linear models, Den Hartog [30] analytically derived the well known optimal tuning parameters for a tuned mass damper added to an undamped base system.

$$\zeta_{opt} = \sqrt{\frac{3\mu}{8(1+\mu)^3}} \quad (1)$$

$$f_{opt} = \frac{1}{1+\mu}$$

Optimal design equations and tables considering a damped base system have also been investigated in the literature [31][32].

Increasing computational power has allowed investigation into parameter optimization for nonlinear springs and dampers in a tuned mass damper application [33][34], and evaluation of TMD performance with parameter uncertainty or variation[35] [36].

5.1 Equations of Motion, Derivation of Cost Functions

A tuned mass damper system shown in Figure 28 (considering an undamped or very low damping base system $c_1 \approx 0$) can be represented by a 2DOF spring/mass/damper system with the equations of motion shown in Equation 2.

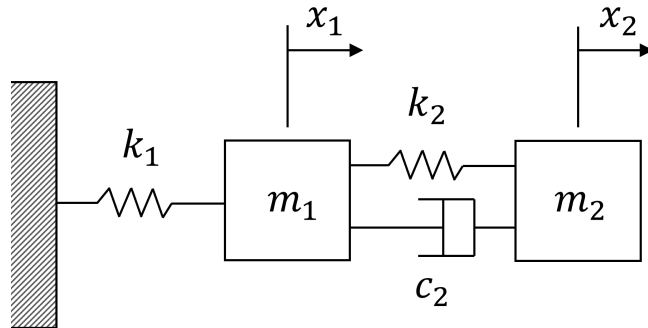


Figure 28: Simplified tuned mass damper diagram

$$m_1\ddot{x}_1 + k_1x_1 - k_2(x_1 - x_2) - c_2(\dot{x}_2 - \dot{x}_1) = F_0 \sin(\Omega t) \quad (2)$$

$$m_2\ddot{x}_2 + k_2(x_1 - x_2) + c_2(\dot{x}_2 - \dot{x}_1) = 0$$

Where m_1, m_2 are the mass of the base system and the tuned mass respectively, where k_1, k_2 are the stiffness of the base system and the tuned mass spring respectively, c_2 is the damping rate of the tuned mass damping element, x_1, x_2 are the displacements of the base system and tuned mass respectively. The input to the base system is considered to be sinusoidal with an input magnitude of F_0 and an input frequency of Ω .

The steady state solution to these equations is well known [37].

$$X_1 = \frac{F_0(k_2 - m_2\Omega^2 + i\omega_2\Omega)}{[(k_1 - m_1\Omega^2)(k_2 - m_2\Omega^2) - m_2k_2\Omega^2] + i\omega_2(k_1 - m_1\Omega^2 - m_2\Omega^2)} \quad (3)$$

$$X_2 = \frac{X_1(k_2 + i\omega_2\Omega)}{(k_2 - m_2\Omega^2 + i\omega_2\Omega)} \quad (4)$$

Defining

$$\mu = m_2/m_1 \quad (\text{mass ratio})$$

$$\omega_1 = \sqrt{k_1/m_1} \quad (\text{natural frequency of mass 1})$$

$$\omega_2 = \sqrt{k_2/m_2} \quad (\text{natural frequency of mass 2})$$

$$f = \omega_1/\omega_2 \quad (\text{TMD frequency ratio})$$

$$g = \Omega/\omega_1 \quad (\text{Forcing frequency ratio})$$

$$\zeta = c_2/(2\sqrt{m_2k_2}) \quad (\text{TMD damping ratio})$$

$$\delta_s t = F_0/k_1 \quad (\text{mass 1 static deflection})$$

Normalized vibration magnitude for the main mass can be defined as in Equation 5, with normalized vibration magnitude in Equation 6 with the optimal parameters of Equation 1.

$$\left| \frac{X_1}{\delta_s t} \right| = \sqrt{\frac{(2\zeta g)^2 + (g^2 - f^2)^2}{(2\zeta g)^2(g^2 - 1 + \mu g^2)^2 + (\mu f^2 g^2 - (g^2 - 1)(g^2 - f^2))^2}} \quad (5)$$

$$\left| \left(\frac{X_1}{\delta_s t} \right)_{opt} \right| = \sqrt{1 + 2/\mu} \quad (6)$$

In traditional tuned mass damper design, the parameters m_1 , k_1 and Ω are fixed as characteristics of the base system that has undesirable vibration/motion at a particular frequency. The parameters that are “tuned” to maximize the effectiveness are m_2 , k_2 and c_2 .

5.2 Frequency Uncertainty for Robust Performance

In the design and manufacturing of any mechanism, there exist manufacturing tolerances and variance in construction. Even if a well modeled, correlated simulation of the system to be built exists, these natural variations may make the behavior of a large number of the manufactured product vary in their performance compared to the simulation. In the context of this thesis, there are many sources of possible variance that could cause a ball bonder rear Y slide and a tuned mass damper mounted to it to not behave as modeled originally.

Changes in material properties from batch to batch are expected when dealing with viscoelastic materials. Assembly of mechanical structures with threaded fasteners is also prone to variance through differences in tightening torque. Even with use of calibrated

tools like torque wrenches, variance in bolt preload possibly as high as $\pm 20\%$ could still exist.

In the context of a moving XY table assembly with mechanical bearings, the support offered by the bearings will change as the moving mass traverses its available working space, which will change the vibration modes of the structure. This can be seen in Figure 10. Additionally, build variation in individual bearing interfaces will show small differences in natural frequency and damping of critical modes as the bearings wear over the lifetime of axis.

In the context of structures with a coefficient of thermal expansion mismatch between components (such as an aluminum structure with steel bearings bolted on), there also exists thermal sensitivities that will change the response of the system much more than the very small change in Young's Modulus of common engineering metals across a $20-30^{\circ}\text{C}$ temperature delta if preload or bearing alignment changes due to thermal expansion.

For these reasons, it is highly desirable to understand the robustness and sensitivity of a tuned mass damper design to changes in the base system or tuned mass damper natural frequency and damping. Robust design of TMD parameters has been investigated in the literature[38][39][40], but has not progressed to the point of having a simple to use design formulas or charts for use in selecting optimal parameters for a specific TMD design. In the application on a ball bonder, "re-tuning" of a TMD is not feasible due to cost and uptime considerations. To evaluate the robustness and sensitivity of a TMD system, a set of MATLAB scripts were made to evaluate the equations of motions across a wide range of conditions.

The simplicity of the simple TMD model lends itself to simple optimization routines. With modern computing power, more computationally efficient optimization routines are often not needed due to the programming/setup time investment. For these reasons, a

simple “brute force” type routine with the following steps was used to evaluate all possible design parameter combinations.

1. Define a range of frequency uncertainty and search ranges and intervals for frequency ratio and damping ratio
2. Compute Equation 5 for a range of forcing frequency ratio from 0.5 to 1.5.
3. Record the peak value of the computed Equation 5 for this combination of damping ratio, TMD frequency, and base system frequency.
4. Plot the peak values on a surface plot, identify minimum point on surface and print the optimal parameters at that minimum point

An example of the response surface generated by the MATLAB code is shown in Figure 29.

5.3 Design Curves for Common Mass Ratios

A series of peak optimal design curves in Figure 31 and Figure 30 were created using the developed MATLAB scripts to allow for quick design and tuning of future TMDs that are robust against parameter variation. Interpolation for different mass ratios will give satisfactory results. Also shown in Figure 32 is a normalized performance tradeoff plot, where the vibration reduction performance of an optimal TMD with no mis-tuning per Equation 6 is normalized as 1. It is known that tuned mass dampers are sensitive to proper tuning so the poor performance of mistuning is not surprising.

Polynomial fits for damping ratio and frequency ratio are listed in the Table 7 and Table 8. Note that for no frequency uncertainty these values converge with traditional TMD optimal parameters.

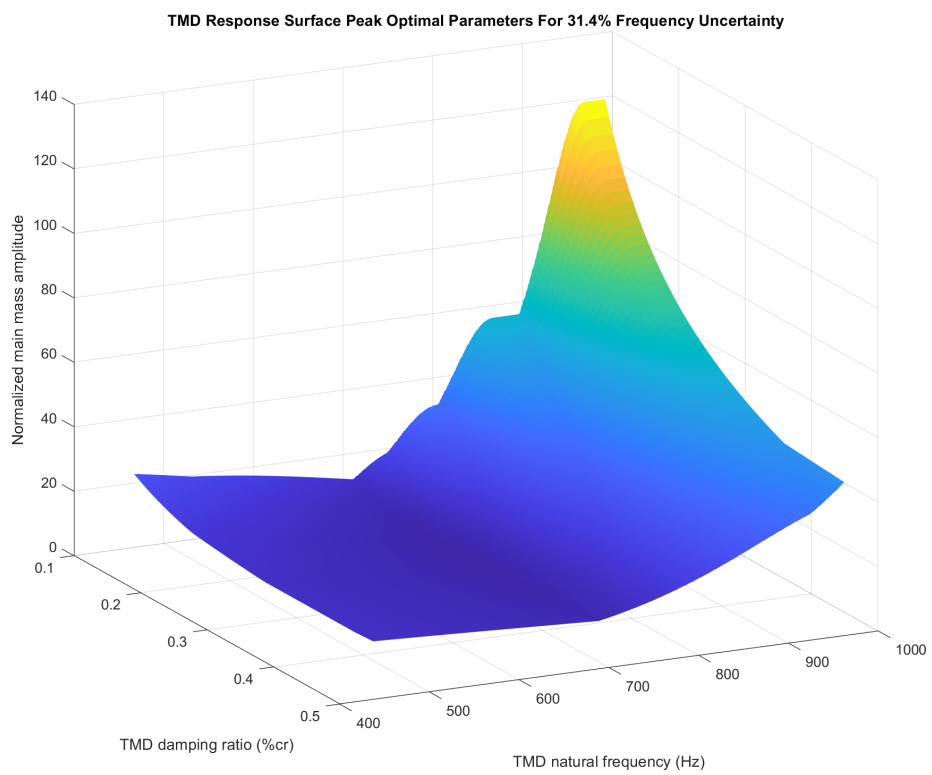


Figure 29: Response surface generated by parameter optimization MATLAB script

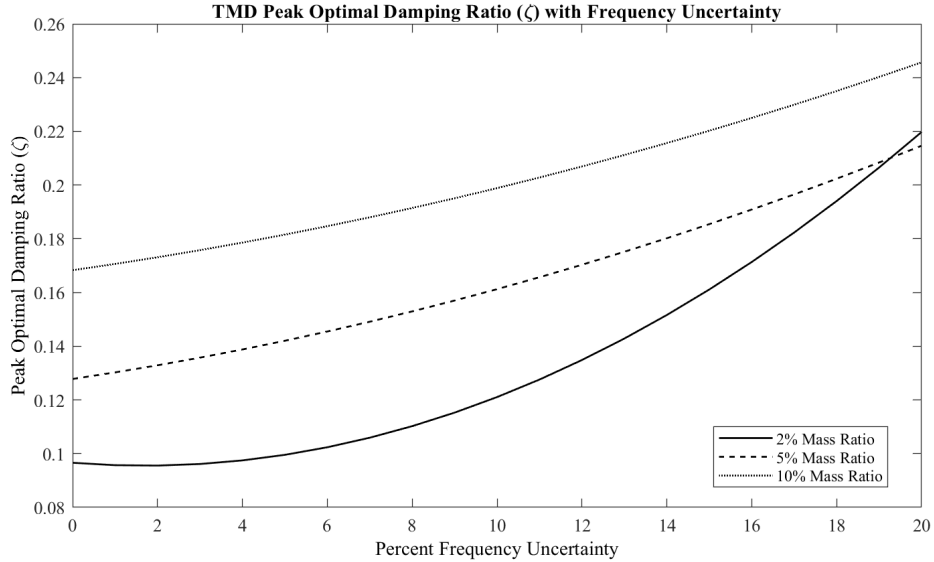


Figure 30: Peak optimal damping ratio curves for different mass ratios

Overall these results match expectations in that more damping on the TMD helps when the base system frequency will change and that higher mass ratios make the system less sensitive to changes in the base system. The well known Lanchester Damper [30], a tuned mass damper, without a spring element and a high damping ratio (typically $\zeta > 0.7$), takes this concept to its logical conclusion and gives a small amount of vibration reduction compared to a TMD, but is effectively insensitive to tuning and gives broadband vibration reduction.

Table 7: Optimal damping ratio fit parameters

Mass Ratio	Quadratic Term	Linear Term	Constant Term
2%	3.710e-4	-1.264e-3	0.0966
5%	9.971e-5	2.347e-3	0.1278
10%	8.124e-5	2.243e-3	0.1683

Table 8: Optimal frequency ratio fit parameters

Mass Ratio	Quadratic Term	Linear Term	Constant Term
2%	-1.280e-4	-2.892e-4	0.9817
5%	-1.341e-4	-4.261e-5	0.9527
10%	-1.202e-4	-2.499e-4	0.9102

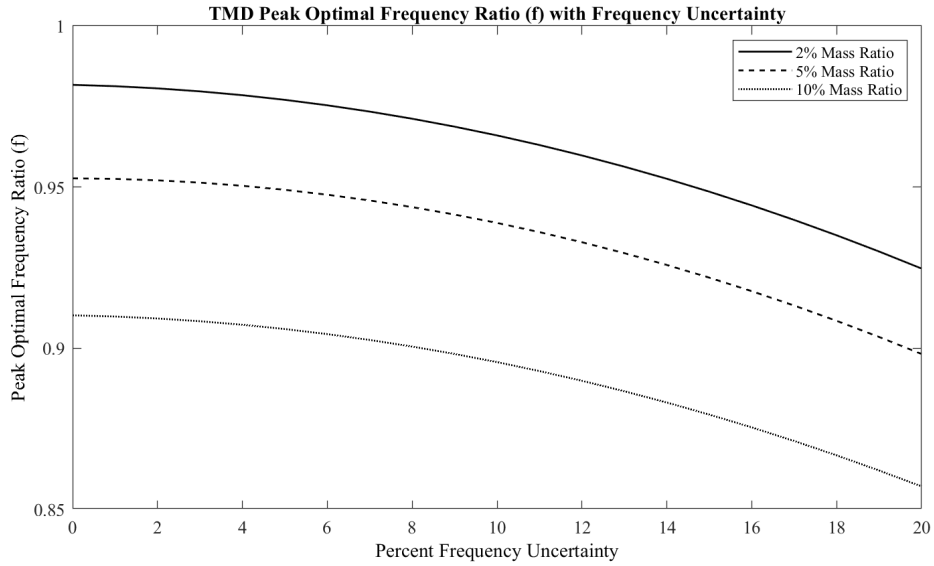


Figure 31: Peak optimal frequency ratio curves for different mass ratios

6 Design, Prototyping, and Testing of Tuned Mass Dampers

With an understanding of the nature of the Rear Y Slide vibration and understanding of optimal design parameters for a TMD, a TMD prototype can be designed. Packaging, desired cost, material properties, and assembly limitations will restrict the possible types of TMD that can be designed. Analysis of individual mass, spring, and damping methods will give a good idea of the possible design space.

6.1 Spring Element Design

The design requirements for the spring element of a Rear Y Slide TMD prescribe a spring that has effectively zero friction, is small and easy to package, and easily adjustable stiffness. For these purposes, a flexure type design is just about the only option, as its properties are easy to modify and can be evaluated quickly with common FEA software.

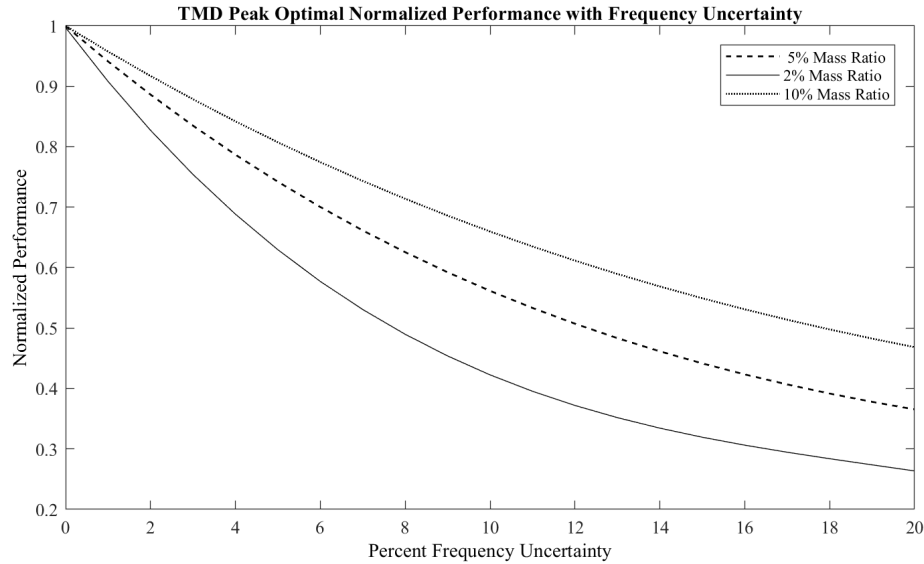


Figure 32: Normalized performance curves for different mass ratios

6.2 Mass Element Design

Mass is often the easiest parameter to design on a tuned mass damper. For packaging and cost reasons, it is desirable to have a high density material for the “tuned” mass. The materials listed in Table 9 were considered due to their high densities and reasonable ease of cost and fabrication. Of these, brass and steel were selected as primary prototyping materials. Brass has a unique combination of low cost, higher density than steel, and more favorable maintainability than steel. Tungsten was selected as a secondary choice; although it has extremely high density, it is expensive and difficult to machine. Lead was eliminated as a choice due to its low stiffness and severe environmental hazard during manufacturing and service.

Table 9: Candidate materials list for tuned mass

Material	Modulus (GPa)	Density (g/cc)
Brass	110	8.5
Mild Steel	200	7.9
Tungsten	400	19.3
Lead	14	11.3

6.3 Damping Source Design

A source of damping is the primary issue in a tuned mass damper when scaled to a size feasible for a semiconductor manufacturing machine. The small scale, approximately linear behavior to damp both large and small vibrations, low mass requirements, and near friction-less operation needed limit the physical mechanisms that can be used for damping.

6.3.1 Fluid/Grease Based Damping

Damping on larger (civil engineering) sized tuned mass damper often comes in a discrete hydraulic damping unit, similar to shock absorbers that are found on cars and motorcycles. A shock absorber style arrangement for this TMD application has issues. The small scale of displacement means that any play, hysteresis, or friction from seals, reservoirs, or moving pistons will be unsuitable. Therefore a zero friction method of damping is needed.

Damping from small gaps between moving parts filled with high viscosity fluid specifically for a tuned mass damper or Lanchester damper application has been investigated with good success in the literature [41].

However, due to increased part count from the need to seal and fill a oil/grease based system, other damping methods were investigated instead.

6.3.2 Eddy Current Damping

Eddy current damping has been investigated in the literature[42][43][44] extensively in applications for a tuned mass damper with success.

In the application on the Rear Y Slide, there exist extremely strong neodymium magnets needed for the linear motor. Eddy current damping was not investigated because the

presence of these magnets could interfere with the operation of the eddy current damper magnets and could cause assembly issues due to the attractive force between the magnets that would require a special assembly fixture method.

6.3.3 Viscoelastic Material Damping

Viscoelastic damping materials are well suited to a TMD application if designed properly. Select rubber-type materials display an extremely high degree of internal material damping also called loss factor (η) [45]. They convert mechanical energy from vibration and displacement into internal heat.

Nomograms of selected commercially available damping materials are shown in Figures 33 and 34. These plots are provided by the manufacturers as a convenient way to display select nonlinear material properties of damping viscoelastic materials..

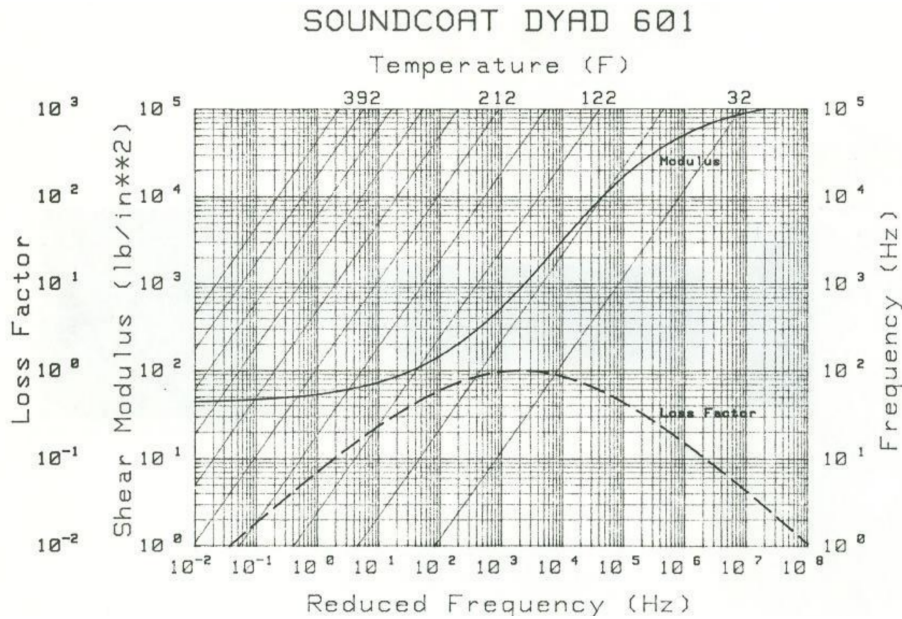


Figure 33: Soundcoat DYAD 601 damping material nomogram

It can be seen from the figures that loss factor and shear stiffness depends heavily on temperature and frequency. From the past modal testing and FE modeling, frequency the

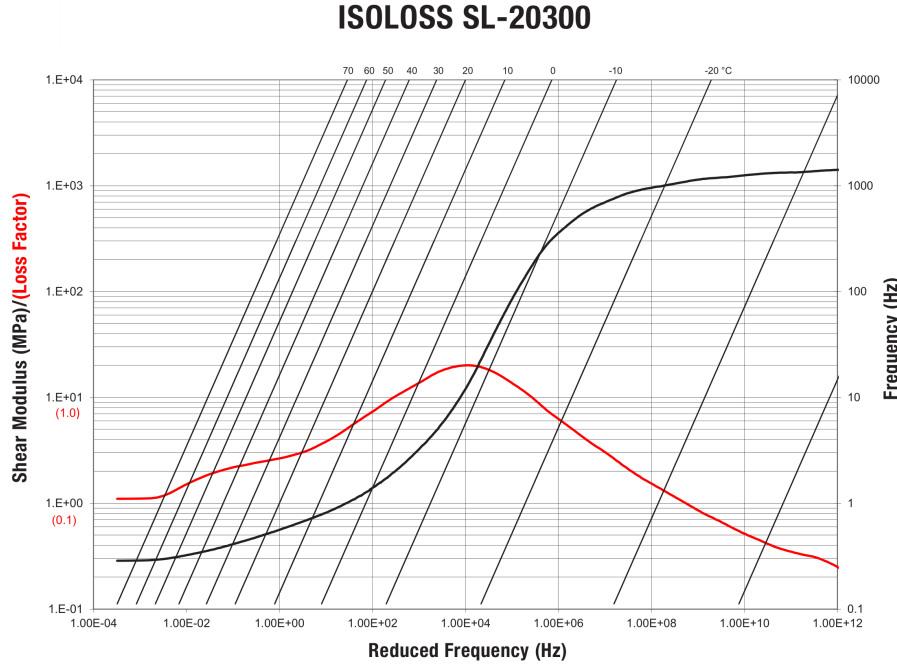


Figure 34: EAR SL20300 damping material nomogram

damping material needs to operate at can be determined. Depending on the specific material blend, critical material parameters can vary by orders of magnitude with only a 10°C change in temperature, so it is critical to select a material with good temperature sensitivity in the region of interest.

Free layer damping is often seen as the simplest possible method to add damping with a viscoelastic layer, as it implies simply adhering damping material on all or part of the part to be damped. While it may not be the most mass efficient option, it is simple to fabricate, simple to analyze, and potentially lower cost compared to damping options that need more complex assembly/manufacturing.

Applying the free-layer damping to a simple beam shown in Figure 35 is easy to evaluate with closed form analytical equations known as “RKU” equations [46]. Equation 7 is an easy to apply closed form equation for evaluating the loss factor of a simple beam treated with free layer damping material.

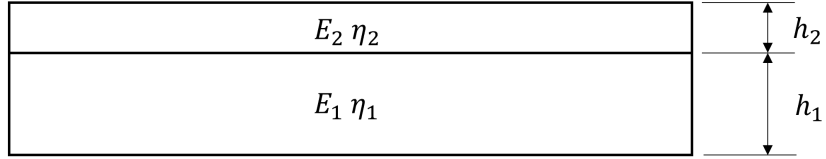


Figure 35: Free layer damping design parameter diagram

The critical design parameters for free layer damping are the stiffness ratio between the damping layer and base structure $e = Re(E_2/E_1)$, and the ratio of height between the damping layer and base structure $h = h_2/h_1$. These combined parameters relate to the fundamental limitation of free layer damping, where the only way to add damping is to have the stiffness of the damping layer contribute significantly to the stiffness of the overall composite structure.

Because most commercial damping material data only provides shear modulus (G) as a function of temperature and frequency, the elastic modulus must be approximated. Most rubbers can be approximated as having a very high Poisson's ratio $\nu \approx 0.5$. From simple solid mechanics for an isotropic material, Elastic modulus is approximated as

$E = 2G(1 + \nu) \approx 3G$. Note that shear modulus is a function of both temperature and frequency.

$$\eta = \eta_2 \frac{eh(3 + 6h + h^2 + 2eh^3 + e^2h^4)}{(1 + eh)(1 + 4eh + 6eh^2 + 4eh^3 + e^2h^4)} \quad (7)$$

The takeaway from Equation 7 is that maximizing the loss factor of the damping material and a high height ratio will give significant damping to the base structure for a given material combination selection. Design curves [46] for this equation from are shown in Figure 36.

From the existing work on the TMD parameter optimization, it is known that damping

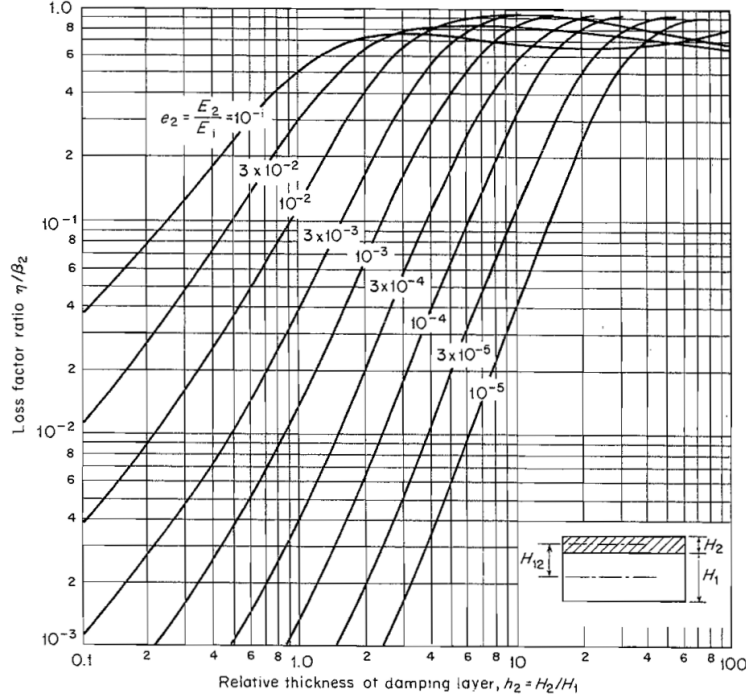


Figure 36: Design chart for free layer damping

ratios of 0.1 to 0.25 are optimal for the mass ratios typically used in TMD design. To see if this range of damping is possible within a reasonable range of flexure material and thickness, calculations were done with commercially available damping materials, different flexure thicknesses, and at different temperatures. The results are shown in Tables 10 and 11. All damping material properties are taken at a nominal 2kHz, as this range is close to the natural frequencies of interest on the Rear Y Slide. Flexure properties are taken to be steel of $E_1 = 203\text{GPa}$ and $\eta_1 = 1 \times 10^{-4} \approx 0$. A flexure thickness of $h_1 = 0.020\text{in}$ will be considered as it is a suitable size in terms of packaging for TMD designs to be discussed later and commercially available as shim stock. For low values of damping $\zeta \approx \eta/2$.

The results of these preliminary calculations indicate that free layer damping could be a suitable damping mechanism, but the design parameters of damping material stiffness and layer thickness are highly sensitive to the overall system loss factor. Exact tuning of

Table 10: Material properties for evaluation of a flexure based free layer damping design

Material	Shear Modulus (G_2 , MPa) at 2kHz, 20°C	Shear Modulus (G_2 , MPa) at 2kHz, 30°C	Loss Factor (η_2) at 2kHz, 20°C	Loss Factor (η_2) at 2kHz, 30°C
EAR SL20300	4.5	2.4	1.6	1.1
SoundCoat DYAD609	414	138	0.21	0.37

Table 11: Example computed loss factors for evaluation of a flexure based free layer damping design. Values in bold indicate viable design parameter combinations within adjustment range for an optimal TMD design

Damping Material	Damping Material Thickness h_2 (in)	System Loss Factor η at 20°C	System Loss Factor η at 30°C
EAR SL20300	0.060	0.019	0.007
EAR SL20300	0.120	0.116	0.044
EAR SL20300	0.180	0.370	0.136
DYAD 609	0.020	0.017	0.010
DYAD 609	0.060	0.223	0.131
DYAD 609	0.100	0.867	0.509

damping ratio might be difficult to attain while using commercially available damping material sheet thicknesses.

6.4 Testing of TMD Designs

Due to the uncertainty in the exact TMD parameters of the designs, 2 iterations of prototypes were fabricated and tested to ensure the modeling results matched the response of the real system.

6.4.1 Design Iteration 1

A first TMD prototype was conceptualized and machined. A photograph of the initial design is shown in Figure 37.

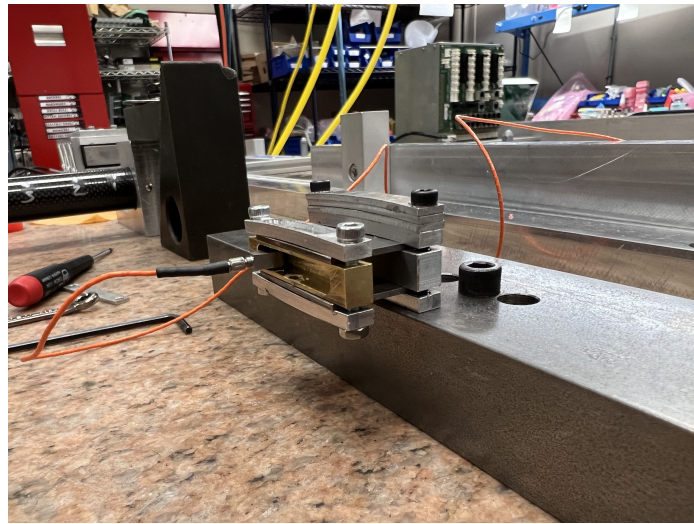


Figure 37: Initial TMD prototype, note bending of clamping mechanism

FEA was used to evaluate the first two natural frequencies of the assembly. Shown in Figure 38, the first natural frequency is close to the target mode natural frequency and free length will be easily adjustable to tune exactly. The second natural frequency is quite high and far away from the range of interest.

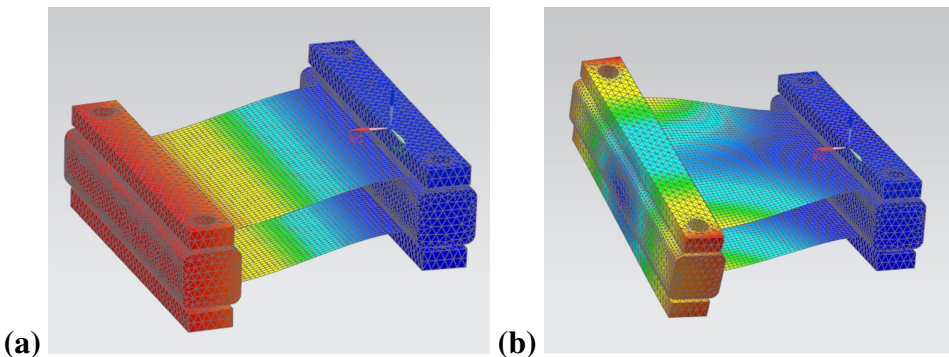


Figure 38: TMD revision 1 natural frequencies (a) first bending mode 1843Hz (b) second twisting mode 4602Hz

A test fixture was machined from steel to test the TMD designs in isolation from the rear Y extrusion.

First, an un-damped design was tested to evaluate the flexibility of the design to “tune” the TMD to desired frequency and damping. The design was found to behave as predicted, in that the natural frequency of the first mode was easily adjustable by repositioning the free

cantilevered length of the flexure, as shown in Figure 40, where each line represents a different cantilever distance of an adjustment range from 1400Hz to 2000Hz. However, the clamping mechanism to clamp the shims was not stiff enough compared to the parts, as major visible deflection was obvious in Figure 37.

To solve this a center bolt and slot were added to the design. Testing with various bolt torques showed that the natural frequency and damping was highly dependent on the bolt torque, as shown in Figure 39. Investigations into bolted joint stiffness and natural frequency has been investigated in the literature [47] and the TMD test results match the general trends. After preliminary investigations into adding damping to this design, the concept was abandoned due to the large amount of vertical space that would be needed to add sufficient damping material for a TMD of this mass ratio and design.

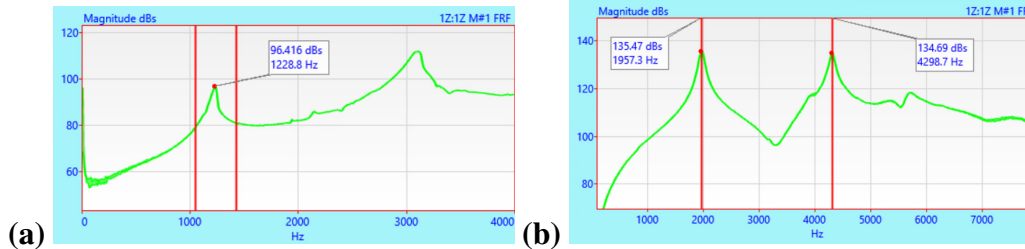


Figure 39: Tap testing FRF data of first TMD design (a) Low bolt tightening torque (b) High bolt tightening torque

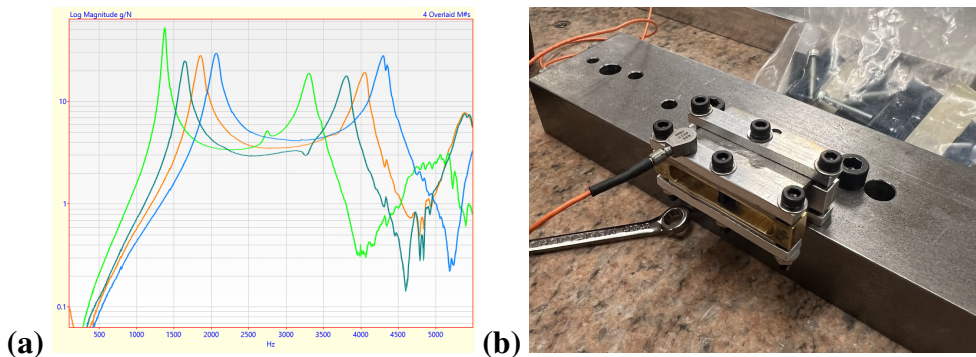


Figure 40: 3 bolt TMD design (a) FRF magnitude data with varying cantilever length (b) Photograph of tap test setup

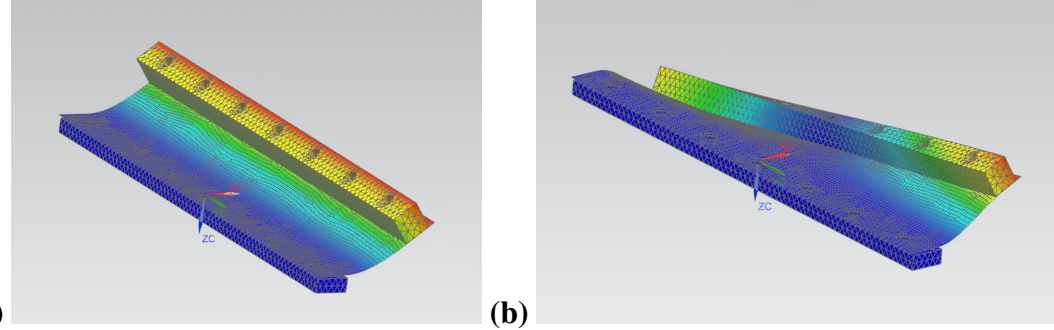


Figure 41: Second TMD design FEA results (a) Mode 1 1897Hz (b) Mode 2 2890Hz

6.4.2 Design Iteration 2

A second TMD design was designed and fabricated to mitigate the issues found in the first design iteration. The primary changes are a smaller, more compact mass that reduces the Z height of the assembly, significantly more fasteners better distributed throughout the part, and a switch to a single shim design. Slots were milled into the shim design to allow for adjustment of the “free length” of the cantilevered section. These combined changes reduced the end mass of the brass and included fasteners assembly to 7.55g. This lower weight would require less damping material to give optimal performance, but would limit the maximum vibration reduction potential of the TMD. FEA was used to select preliminary shim thickness, flexure cantilever distance, and to evaluate the 2nd and higher natural frequencies of the assembly. The results of the FEA shown in Figure 41. The results showed that this design had a lower second natural frequency compared to other designs.

Again a test fixture was machined from steel to test the TMD designs in isolation from the rear Y extrusion. Photographs of the machined and assembled design setup for testing with a laser vibrometer and accelerometer without damping material as setup on the test fixture on a vibration isolated surface plate are shown in Figure 42. Initial testing with no damping material showed very good agreement with FEA results with experimental first

and second natural frequencies measured as 1941.3Hz (2.2 % error) and 2917.3Hz (0.94 % error) respectively.

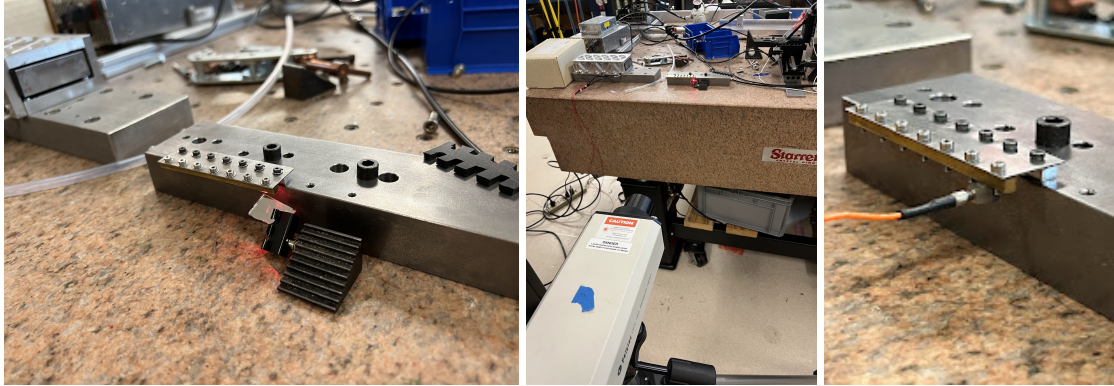


Figure 42: Photographs of the second TMD design revision setup for laser vibrometer and accelerometer testing

Once tuned appropriately with no damping material, EAR SL damping material cut to an appropriate profile was adhered with Permabond 240 CA glue. CA Glue was selected due to its high stiffness and ease of application. From the damping estimates from RKU equations, 2 setups were tested, a 0.060in layer and a 0.120in layer. The addition of the damping material approximately matched the results of the RKU equations. Tap testing with a laser vibrometer allowed for damping and natural frequency to be measured. Damping was evaluated by the half-power bandwidth method [48][49] to approximate the damping . Results of the tap testing are shown in Figure 43.

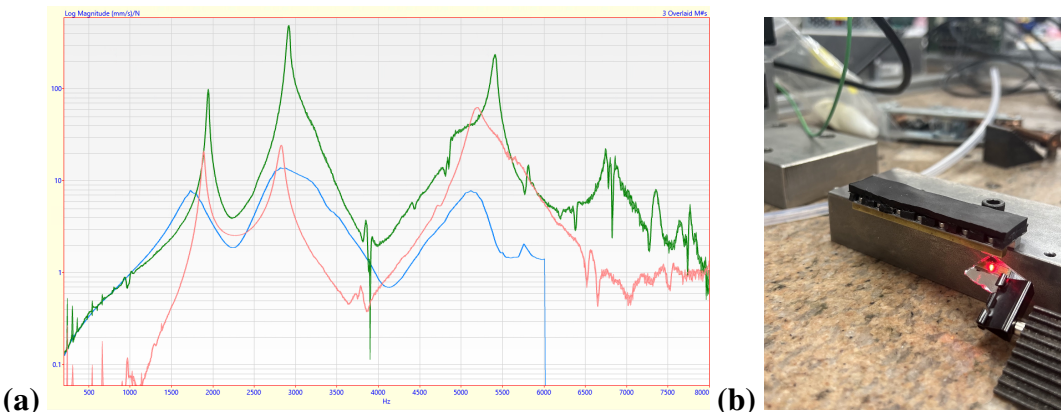


Figure 43: Second TMD design tap testing (a) FRF Magnitude results, (green: no TMD, coral: .060in layer EAR SL, blue: .120in layer EAR SL) (b) Photograph of test setup

With the assembly tuned on the bench, it was moved to a full rear Y assembly to test the effectiveness at suppressing the vibration of the targeted mode. Photographs of the on-bonder test setup are shown in Figure 44. Rear Y extrusion vibration was recorded with a teardrop accelerometer and TMD vibration was recorded with a laser vibrometer. Excitation was provided by an impact hammer tap at the front of the Rear Y extrusion.

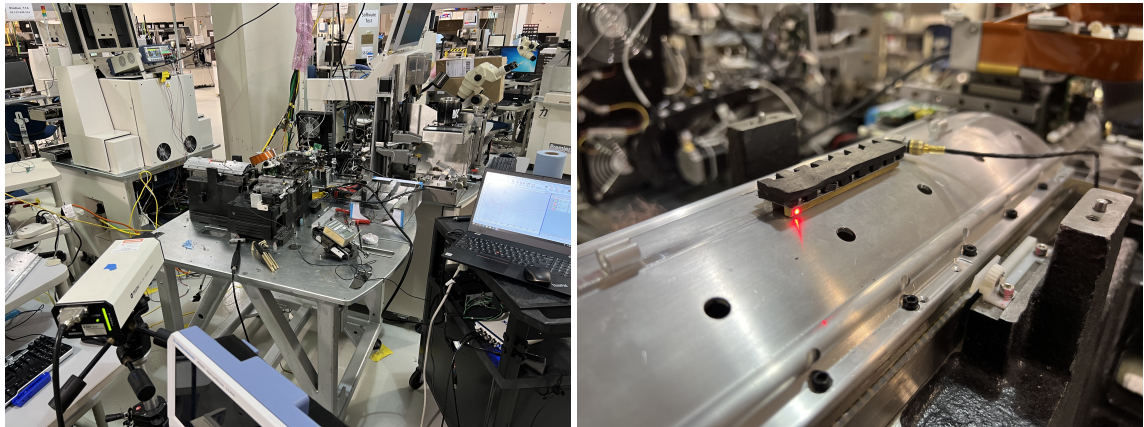


Figure 44: On bonder TMD testing setup photos

The results of the on bonder testing matched the modeling expectations and results from the literature. An un-damped TMD would “split” the peak. Adjusting the frequency tuning of the TMD by modifying the free length or mounting bolt tightening torque could manipulate the heights of each peak. By running multiple tests with small variations in bolt preload, it was easy to tune the frequency of the TMD to minimize the overall measured vibration. The results of the un-damped TMD are shown in the orange lines in Figure 45.

Damping material was added in a similar fashion to the test bench setup. First a .060in layer of EAR SL material was added, second a .120in layer. Again the damper was mounted and tuned in a similar way to the undamped setup. Adding damping to the TMD improved the broadband vibration reduction of the device.

The maximum vibration reduction of 61.4% was found with the .060in layer of EAR SL material, the full results are shown in Table 12. It is assumed that the TMD with 0.120in

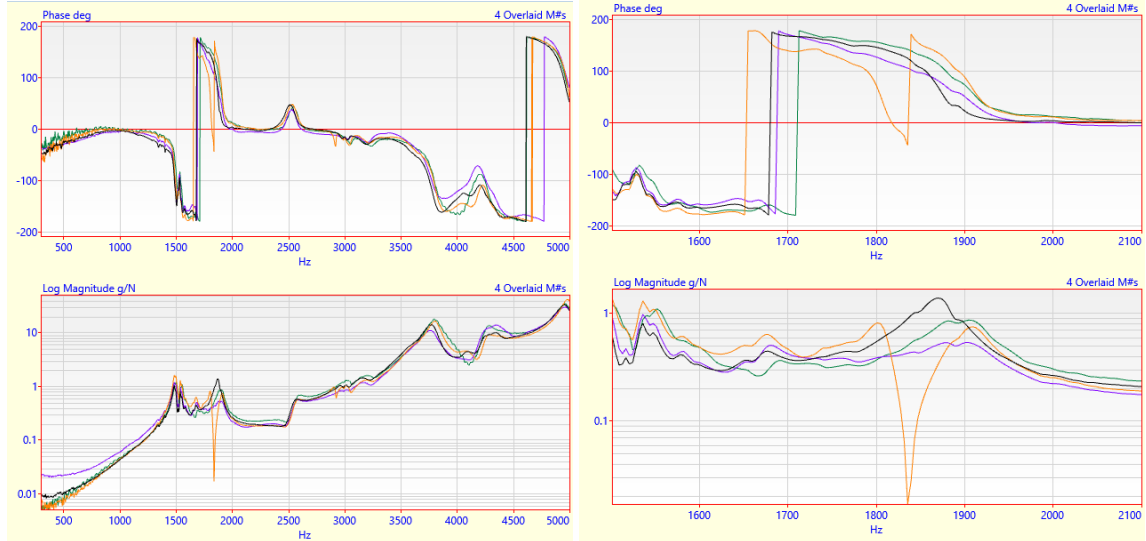


Figure 45: Measured vibration Bode plots with various TMD setups. Right view inset 1700-2100Hz (Black: No TMD, Orange: Un-damped TMD, Purple: TMD with .060in of EAR SL material, Green: TMD with .120in of EAR SL)

of EAR SL material is over-damped for the optimal TMD performance in this condition. This error could come through errors in the effective mass ratios of the TMD assembly. If the effective mass of the TMD results in a lower mass ratio, a lower damping ratio would be needed to reach appropriate tuning. Another possible source for error is a difference in how the damping material was bonded to the TMD assembly. The beneficial effect of an over-damped TMD will be its increase in robustness if the natural frequency of the base system were different.

Table 12: Results summary of on-bonder TMD testing

TMD Setup	Peak FRF Amplitude 1.8-2kHz (g/N)	% Reduction
No TMD	1.3893	-
Un-damped TMD	0.8167	41.2
TMD .060 EAR SL Material	0.5360	61.4
TMD .120 EAR SL Material	0.86612	37.6

7 Future Work and Recommendations

7.1 Summary

This work has investigated the design process of a TMD for use on the Y axis of a high speed XY table assembly in a ball bonder machine. Experimental methods and FEA tools were used characterize the noise and vibration of the assembly of interest. Optimal design parameters were estimated for a TMD solution that would be robust to the parameter variations expected in use of the assembly. Design concepts to realize the TMD were created, and prototypes were fabricated. Prototypes were tested, tuned, and refined to achieve desired performance in bench testing. Tuned designs were then integrated into the Y axis assembly and tested to show the vibration reduction potential of such a device.

7.2 Future Work

This work leaves many opportunities to improve and further quantify the possible benefit of TMD style devices for noise and vibration reduction. A logical extension to the work in this thesis would be to design and tune other TMD devices to target the remaining major vibration modes found in the Rear Y Slide assembly, such as the 900Hz “overhang bending mode”. Multiple TMD systems have found good success in broadband damping of vibration in continuous structures [50] [51]. These TMD devices could use a similar construction and tuning method, or could incorporate a multi-DOF TMD design [52]. Possible downsides of this is the additional complexity and cost from a multiple or more complex TMD solution.

If cost, packaging, and other constraints changed, other damping sources should be investigated. Damping though high viscosity fluids or greases could prove to be a better, more adjustable method for adding damping to a TMD design. Additionally, a composite

viscoelastic damping layer, for example, alternating layers of EAR SL 20300 and Soundcoat DYAD 609, could allow for a TMD to perform more reliably across a wider temperature range due to differences in the change of material properties with temperature.

While the audible noise properties of the Rear Y slide assembly were studied without the addition of the TMD, more testing could be done to quantify the noise reduction potential of the assembly, in bench testing and in the context of a completed machine. Based on the existing work, it is assumed that there will only be minor impacts on the broadband noise reduction potential of the device.

While the temperature dependent properties of both the XY table itself and the damping materials used were discussed, the impact of temperature changes was not measured. The Y axis linear motor itself or a discrete resistive heater and power supply could be used as a heat source for this testing. By running a set of Y axis motions close to the maximum current within the thermal limits of the motor for a time, the Y axis could heat to its maximum steady state temperature, and the performance of the TMD could be re-evaluated.

Lastly, as with most mechanical assemblies, further refinement and integration of the TMD prototypes is possible. Components that are bolted together could instead be machined into a monolithic assembly or instead bonded with adhesives to reduce part count, labor, and potential for error. For example, the single cantilevered steel flexure design with a bolted brass mass could be combined into to single piece steel design combining both the flexure and mass elements. The aluminum spacer needed to raise the TMD off the rear Y slide extrusion could be a feature directly extruded and post machined.

List of References

- [1] D. A. DeAngelis, “Ultrasonic transducer systems including tuned resonators, equipment including such systems, and methods of providing the same,” U.S. Patent US11 011 492B2, 2021. [Online]. Available: <https://patents.google.com/patent/US11011492B2>
- [2] R. Kyomasu, H. Urabayashi, M. Torihata, K. Takahashi, and T. Miyahara, “Xy table for semiconductor manufacturing apparatus,” U.S. Patent US6 727 666B2, 2004. [Online]. Available: <https://patents.google.com/patent/US6727666B2>
- [3] E. Rivin, H. Kang, and L. Kops, “Improving dynamic performance of cantilever boring bars,” *CIRP Annals*, vol. 38, no. 1, pp. 377–380, 1989. [Online]. Available: [https://doi.org/10.1016/S0007-8506\(07\)62727-9](https://doi.org/10.1016/S0007-8506(07)62727-9)
- [4] A. Aliakbari, G. Moraru, P. Veron, and Y. Groll, “The effect of a polymer-based tuned mass damper on the vibration characteristics of an anti-vibration boring bar,” *Procedia CIRP*, vol. 103, pp. 200–206, 2021, 9th CIRP Global Web Conference – Sustainable, resilient, and agile manufacturing and service operations : Lessons from COVID-19. [Online]. Available: <https://www.sciencedirect.com/science/article/pii/S2212827121008738>
- [5] W. Ma, J. Yu, Y. Yang, and Y. Wang, “Optimization and tuning of passive tuned mass damper embedded in milling tool for chatter mitigation,” *Journal of Manufacturing and Materials Processing*, vol. 5, no. 1, 2021. [Online]. Available: <https://doi.org/10.3390/jmmp5010002>
- [6] W. Ma, Y. Yang, and X. Jin, “Chatter suppression in micro-milling using shank-mounted two-dof tuned mass damper,” *Precision Engineering*, vol. 72, pp. 144–157, 2021. [Online]. Available: <https://doi.org/10.1016/j.precisioneng.2021.04.017>
- [7] Y. Altintas, D. Lappin, D. van Zyl, and D. Östling, “Automatically tuned boring bar system,” *CIRP Annals*, vol. 70, no. 1, pp. 313–316, 2021. [Online]. Available: <https://doi.org/10.1016/j.cirp.2021.04.058>
- [8] M. Fallah and B. Moetakef-Imani, “Analytical prediction of stability lobes for passively damped boring bars,” *Journal of Mechanics*, vol. 33, no. 5, p. 641–654, 2017. [Online]. Available: <https://doi.org/10.1017/jmech.2017.22>
- [9] A. Patel, D. kumar Talaviya, M. Law, and P. Wahi, “Optimally tuning an absorber for a chatter-resistant rotating slender milling tool holder,” *Journal of Sound and Vibration*, vol. 520, p. 116594, 2022. [Online]. Available: <https://doi.org/10.1016/j.jsv.2021.116594>

- [10] A. Astarloa, M. H. Fernandes, I. Mancisidor, J. Munoa, and Z. Dombovari, “Prediction of the dynamic stiffness of boring bars,” *IOP Conference Series: Materials Science and Engineering*, vol. 1193, no. 1, p. 012007, oct 2021. [Online]. Available: <https://doi.org/10.1088/1757-899x/1193/1/012007>
- [11] A. Bansal and M. Law, “A receptance coupling approach to optimally tune and place absorbers on boring bars for chatter suppression,” *Procedia CIRP*, vol. 77, pp. 167–170, 2018, 8th CIRP Conference on High Performance Cutting (HPC 2018). [Online]. Available: <https://doi.org/10.1016/j.procir.2018.08.267>
- [12] R. W. New and Y. H. J. Au, ““Chatter-Proof” Overhang Boring Bars—Stability Criteria and Design Procedure for a New Type of Damped Boring Bar,” *Journal of Mechanical Design*, vol. 102, no. 3, pp. 611–618, 07 1980. [Online]. Available: <https://doi.org/10.1115/1.3254793>
- [13] Y. Yang, J. Muñoa, and Y. Altintas, “Optimization of multiple tuned mass dampers to suppress machine tool chatter,” *International Journal of Machine Tools and Manufacture*, vol. 50, no. 9, pp. 834–842, 2010. [Online]. Available: <https://doi.org/10.1016/j.ijmachtools.2010.04.011>
- [14] M. F. Heertjes, M. L. van de Ven, and R. Kamidi, “Acceleration-snap feedforward scheme for a motion system with viscoelastic tuned-mass-damper,” in *2017 American Control Conference (ACC)*, May 2017, pp. 2888–2893.
- [15] C. Verbaan, P. Rosielle, and M. Steinbuch, “Broadband damping of non-rigid-body resonances of planar positioning stages by tuned mass dampers,” *Mechatronics*, vol. 24, no. 6, pp. 712–723, 2014, control of High-Precision Motion Systems. [Online]. Available: <https://doi.org/10.1016/j.mechatronics.2013.12.013>
- [16] C. A. M. Verbaan, “Robust mass damper design for bandwidth increase of motion stages,” Ph.D. dissertation, Technische Universiteit Eindhoven, 2015. [Online]. Available: https://pure.tue.nl/ws/files/20530101/20160420_Verbaan.pdf
- [17] K. Verbaan, S. van der Meulen, and M. Steinbuch, “Broadband damping of high-precision motion stages,” *Mechatronics*, vol. 41, pp. 1–16, 2017. [Online]. Available: <https://doi.org/10.1016/j.mechatronics.2016.10.014>
- [18] J. Mathews, *Guide to Adhesively Mounting Accelerometers*, Endevco, 10869 NC Highway 903, Halifax, NC 27839 USA, 2022, technical paper 312.
- [19] (2022) Acoustic simulation. Siemens. [Online]. Available: <https://www.plm.automation.siemens.com/global/en/products/simulation-test/acoustic-simulation.html>
- [20] K. Inoue, M. Yamanaka, and M. Kihara, “Optimum Stiffener Layout for the Reduction of Vibration and Noise of Gearbox Housing ,” *Journal of Mechanical Design*, vol. 124, no. 3, pp. 518–523, 08 2002. [Online]. Available: <https://doi.org/10.1115/1.1480817>

- [21] *Linear Bearings and Recirculating Units*, Schneeberger Linear Technology, September 2021. [Online]. Available: https://www.schneeberger.com/fileadmin/documents/downloadcenter/01_product_catalogues_company_brochures/01_Linear_and_profiled_guideways/03_Linear_bearings_and_recirculating_units/Linearbearings_-_Product_catalogue_EN.pdf
- [22] B. Nelson Norden, “On the compression of a cylinder contact with a plane surface,” National Bureau of Standards, Tech. Rep. NBSIR 73-243, July 1973. [Online]. Available: https://www.nist.gov/system/files/documents/calibrations/nbsir_73-243.pdf
- [23] L. Molnár, K. Váradi, G. Bódai, P. Zwierczyk, and L. Oroszváry, “Simplified modeling for needle roller bearings to analyze engineering structures by fem,” *Periodica Polytechnica Mechanical Engineering*, vol. 54, no. 1, p. 27–33, 2011. [Online]. Available: <https://pp.bme.hu/me/article/view/1266>
- [24] A. H. Slocum, *Precision machine design*. Englewood Cliffs, N.J.: Prentice Hall, 1992, pp. 473–474.
- [25] E. Bamberg, “Modeling bearings for selection and analysis,” Powerpoint slides, 2006. [Online]. Available: <https://my.mech.utah.edu/~me7960/lectures/Topic9-ModelingBearingsForSelectionAndAnalysis.pdf>
- [26] R. G. Budynas, J. K. Nisbett, and J. E. Shigley, *Shigley’s mechanical engineering design*, 2015, pp. 419–422.
- [27] J. Wileman, M. Choudhury, and I. Green, “Computation of member stiffness in bolted connections,” *Journal of Mechanical Design*, vol. 113, pp. 432–437, 1991.
- [28] Y. Ito, J. Toyoda, and S. Nagata, “Interface Pressure Distribution in a Bolt-Flange Assembly,” *Journal of Mechanical Design*, vol. 101, no. 2, pp. 330–337, 04 1979. [Online]. Available: <https://doi.org/10.1115/1.3454058>
- [29] T. Irvine. (2012, November) Bending frequencies of beams, rods, and pipes. 136 Wellington Dr. Madison, Alabama 35758. [Online]. Available: <https://www.vibrationdata.com/tutorials2/beam.pdf>
- [30] J. P. D. Hartog. (2013) Mechanical vibrations. Newburyport. [Online]. Available: <https://www.worldcat.org/title/mechanical-vibrations/oclc/1058607089>
- [31] H. C. Tsai and G.-C. Lin, “Explicit formulae for optimum absorber parameters for force-excited and viscously damped systems,” *Journal of Sound and Vibration*, vol. 176, pp. 585–596, October 1994. [Online]. Available: <https://doi.org/10.1006/JSVI.1994.1400>
- [32] S. V. Bakre and R. S. Jangid, “Optimum parameters of tuned mass damper for damped main system,” *Structural Control and Health Monitoring*, vol. 14, no. 3, pp. 448–470, 2007. [Online]. Available: <https://doi.org/10.1002/stc.166>

- [33] M. Wang, T. Zan, Y. Yang, and R. Fei, “Design and implementation of nonlinear tmd for chatter suppression: An application in turning processes,” *International Journal of Machine Tools and Manufacture*, vol. 50, no. 5, pp. 474–479, 2010. [Online]. Available: <https://doi.org/10.1016/j.ijmachtools.2010.01.004>
- [34] J. Bian and X. Jing, “A nonlinear x-shaped structure based tuned mass damper with multi-variable optimization (x-absorber),” *Communications in Nonlinear Science and Numerical Simulation*, vol. 99, p. 105829, 2021. [Online]. Available: <https://www.sciencedirect.com/science/article/pii/S1007570421001404>
- [35] H. Jensen, M. Setareh, and R. Peek, “Tmds for vibration control of systems with uncertain properties,” *Journal of Structural Engineering*, vol. 118, no. 12, pp. 3285–3296, 1992. [Online]. Available: [https://doi.org/10.1061/\(ASCE\)0733-9445\(1992\)118:12\(3285\)](https://doi.org/10.1061/(ASCE)0733-9445(1992)118:12(3285))
- [36] C. Papadimitriou, L. S. Katafygiotis, and S.-K. Au, “Effects of structural uncertainties on tmd design: A reliability-based approach,” *Journal of Structural Control*, vol. 4, no. 1, pp. 65–88, 1997. [Online]. Available: <https://doi.org/10.1002/stc.4300040108>
- [37] S. S. Rao and P. Griffin, *Mechanical vibrations 6th ed. in SI units.* Harlow Pearson, 2018, ch. 9.11, pp. 891–894.
- [38] H. Yu, F. Gillot, and M. Ichchou, “Reliability based robust design optimization for tuned mass damper in passive vibration control of deterministic/uncertain structures,” *Journal of Sound and Vibration*, vol. 332, no. 9, pp. 2222–2238, 2013. [Online]. Available: <https://doi.org/10.1016/j.jsv.2012.12.014>
- [39] A. Mohtat and E. Dehghan-Niri, “Generalized framework for robust design of tuned mass damper systems,” *Journal of Sound and Vibration*, vol. 330, no. 5, pp. 902–922, 2011. [Online]. Available: <https://doi.org/10.1016/j.jsv.2010.09.007>
- [40] C.-C. Lin, G.-L. Lin, and K.-C. Chiu, “Robust design strategy for multiple tuned mass dampers with consideration of frequency bandwidth,” *International Journal of Structural Stability and Dynamics*, vol. 17, no. 01, p. 1750002, 2017. [Online]. Available: <https://doi.org/10.1142/S021945541750002X>
- [41] C. A. M. Verbaan, G. W. M. Peters, and M. Steinbuch, “Linear viscoelastic fluid characterization of ultra-high-viscosity fluids for high-frequency damper design,” *Rheologica Acta*, vol. 54, no. 8, pp. 667–677, Aug 2015. [Online]. Available: <https://doi.org/10.1007/s00397-015-0862-y>
- [42] W. Wang, D. Dalton, X. Hua, X. Wang, Z. Chen, and G. Song, “Experimental study on vibration control of a submerged pipeline model by eddy current tuned mass damper,” *Applied Sciences*, vol. 7, no. 10, 2017. [Online]. Available: <https://www.mdpi.com/2076-3417/7/10/987>

- [43] J.-S. Bae, J.-H. Hwang, D.-G. Kwag, J. Park, and D. J. Inman, “Vibration suppression of a large beam structure using tuned mass damper and eddy current damping,” *Shock and Vibration*, vol. 2014, p. 893914, May 2014. [Online]. Available: <https://doi.org/10.1155/2014/893914>
- [44] Z. Wang, Z. Chen, and J. Wang, “Feasibility study of a large-scale tuned mass damper with eddy current damping mechanism,” *Earthquake Engineering and Engineering Vibration*, vol. 11, no. 3, pp. 391–401, Sep 2012. [Online]. Available: <https://doi.org/10.1007/s11803-012-0129-x>
- [45] C. Bert, “Material damping: An introductory review of mathematic measures and experimental technique,” *Journal of Sound and Vibration*, vol. 29, no. 2, pp. 129–153, 1973. [Online]. Available: [https://doi.org/10.1016/S0022-460X\(73\)80131-2](https://doi.org/10.1016/S0022-460X(73)80131-2)
- [46] E. Ungar and J. Zapfe, *Noise and Vibration Control Engineering*. Wiley, 2005, ch. 14, pp. 579–609. [Online]. Available: <https://doi.org/10.1002/9780470172568.ch14>
- [47] Y. Zhao, C. Yang, L. Cai, W. Shi, and Y. Hong, “Stiffness and damping model of bolted joints with uneven surface contact pressure distribution,” *Strojniški vestnik - Journal of Mechanical Engineering*, vol. 62, no. 11, pp. 665–677, 2016. [Online]. Available: <https://doi.org/10.5545/sv-jme.2016.3410>
- [48] J.-T. Wang, F. Jin, and C.-H. Zhang, “Estimation error of the half-power bandwidth method in identifying damping for multi-dof systems,” *Soil Dynamics and Earthquake Engineering*, vol. 39, pp. 138–142, 2012. [Online]. Available: <https://www.sciencedirect.com/science/article/pii/S0267726112000528>
- [49] G. Papagiannopoulos and G. Hatzigeorgiou, “On the use of the half-power bandwidth method to estimate damping in building structures,” *Soil Dynamics and Earthquake Engineering - SOIL DYNAM EARTHQUAKE ENG*, vol. 31, pp. 1075–1079, 07 2011. [Online]. Available: <http://dx.doi.org/10.1016/j.soildyn.2011.02.007>
- [50] S. Elias, V. Matsagar, and T. Datta, “Effectiveness of distributed tuned mass dampers for multi-mode control of chimney under earthquakes,” *Engineering Structures*, vol. 124, pp. 1–16, 2016. [Online]. Available: <https://doi.org/10.1016/j.engstruct.2016.06.006>
- [51] J. M. Verdirame, “Design of multi-degree-of-freedom tuned-mass dampers using perturbation techniques,” Ph.D. dissertation, Massachusetts Institute of Technology, 2003.
- [52] W. Ma, Y. Yang, and J. Yu, “General routine of suppressing single vibration mode by multi-dof tuned mass damper: Application of three-dof,” *Mechanical Systems and Signal Processing*, vol. 121, pp. 77–96, 2019. [Online]. Available: <https://doi.org/10.1016/j.ymssp.2018.11.010>

Appendix

A Investigation of Non-TMD Noise/Vibration Control Solutions

For completeness and comparison to a TMD type solution, other noise control solutions were investigated in parallel to the work discussed in this thesis.

A.1 Addition of Damping/Acoustic Material

Products are commercially available targeted at reducing panel noise/vibration, they are typically applied to sheet metal housing and automotive body panels. A tap test of 19 XYZ accelerometer points was conducted with some of this material bonded on to see the impact it would have, the results are shown in Figure 47. A photo of the applied material is shown in Figure 46. Overall the addition of the material added significant mass to the structure, this reduced natural frequencies. No significant increase in damping was found.



Figure 46: Commercially available damping material adhered to Rear Y

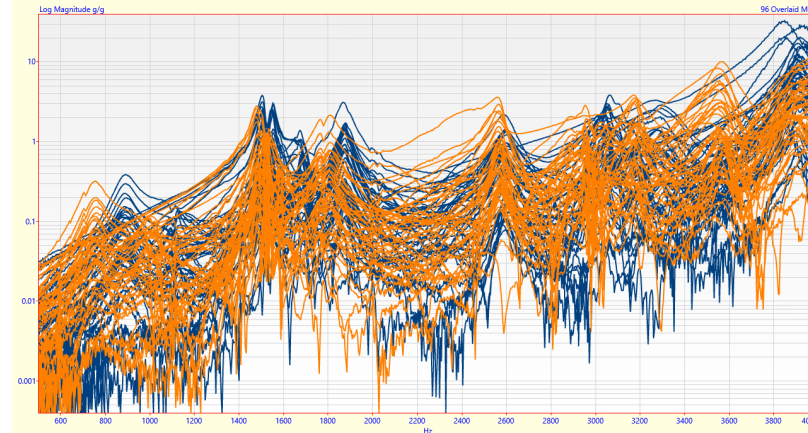


Figure 47: Tap testing results of a Rear Y slide with damping material (orange) compared to a baseline Rear Y Slide (navy blue)

A.2 Increasing Stiffness by Bonding Components

From the FEA results in section 4, it was known that the connection between the magnetway component and aluminum extrusion could be improved.

To investigate this concept, FEA and empirical testing were carried out to see if adding an epoxy layer to bond the two components would both increase natural frequencies and damping of key noise producing modes.

To test empirically, a magnetway component was bolted and bonded to a rear Y slide extrusion with Loctite E-20HP structural epoxy, a photograph of the bonded assembly is shown in Figure 48. The bonded structure was assembled onto a ball bonder XY table and tap tested to compare to a non-bonded setup, the results are shown in Figure 49. Overall the results matched the FEA results, but with less of an increase in natural frequencies as the stiffness of the epoxy was not accounted for in the FEA. Unfortunately, the results appear to show a decrease in damping of key modes.



Figure 48: Photo of epoxy bonding layer between Rear Y Slide extrusion and magnetway

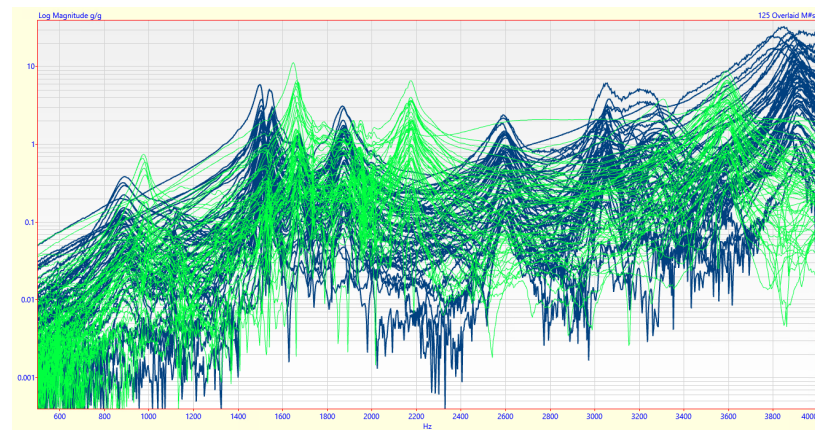


Figure 49: Tap testing results of a Rear Y slide with epoxy bonding (green) compared to a baseline Rear Y Slide (navy blue)

B MATLAB Code for TMD Parameter Optimization

```

1 %% TMD optimization with Frequency Uncertainty
2 % David Haruch, 03/2022
3
4 % properties of system TMD will be attached to
5 str_min_freq = 600;
6 str_max_freq = 1150;
7 str_mid_freq = (str_max_freq+str_min_freq)/2;
8 percent_freq_variability = (str_max_freq-
      str_mid_freq)/str_mid_freq
9
10 % search range for optimal TMD parmaeters
11 TMD_min_freq = str_mid_freq*0.5;
12 TMD_max_freq = str_mid_freq*1.1;
13 TMD_freq_range = TMD_min_freq:1.1:TMD_max_freq;
14 TMD_damp_range = 0.14:.006:0.5;
15 mass_ratio = 0.1;
16
17 df = .1;
18 freq_ratio_range =
      (TMD_min_freq/str_max_freq):df:(TMD_max_freq/str_min_freq);
19 nom_TMD_freq = freq_ratio_range.*str_mid_freq;
20
21 ratio_test_range = 0.5:.01:1.5;
22
23 % sweep the TMD freq and damping range for each incremenet of
      mistuning & store in array
24 % generate summary statistics (average amp, RMS amp, max
25
26 results_arr_avg =
      zeros(length(freq_ratio_range),length(TMD_damp_range));
27 results_arr_rms =
      zeros(length(freq_ratio_range),length(TMD_damp_range));
28 results_arr_pk =
      zeros(length(freq_ratio_range),length(TMD_damp_range));
29
30
31 bar = waitbar(0,'Processing','Units','normalized');
32
33 for i=1:length(TMD_freq_range)
34   for j=1:length(TMD_damp_range)
35
36     this_TMD_freq = TMD_freq_range(i);
37     progress = this_TMD_freq/TMD_max_freq;
38     waitbar(progress,bar)

```

```

39
40 low_ratio = this_TMD_freq/str_min_freq;
41 hi_ratio = this_TMD_freq/str_max_freq;
42 ratios = [low_ratio hi_ratio];
43
44 this_ratio_range = min(ratios):0.002:max(ratios);
45
46 % compute the objective function
47 A_max = zeros(size(this_ratio_range));
48 for k=1:length(this_ratio_range)
49 f = this_ratio_range(k);
50 c = TMD_damp_range(j);
51 g = ratio_test_range;
52 top = (2.*c.*g).^2 + (g.^2 - f.^2).^2;
53 bottom = (2.*c.*g).^2.*((g.^2 - 1) + mass_ratio.*g.^2).^2 + (
    mass_ratio.*f.^2.*g.^2 - (g.^2 - 1).*((g.^2 - f.^2))).^2;
54 A = sqrt(top./bottom); % Array of all amplitudes for a given
    damping ratio/freq
55 A_max(k) = max(A); % this is objective function value
56 end
57 results_arr_pk(i,j) = max(A_max);
58 results_arr_avg(i,j) = mean(A_max);
59 results_arr_rms(i,j) = rms_function(A_max);
60
61 end
62 end
63
64 %% post processing
65
66 norm_results_arr_avg = results_arr_avg./min(min(results_arr_avg));
67 norm_results_arr_pk = results_arr_pk./min(min(results_arr_pk));
68 norm_results_arr_rms = results_arr_rms./min(min(results_arr_rms));
69
70 % extract optimal parameters for each case
71
72 %pk only for now
73 [M,I] = min(results_arr_pk,[],'all','linear'); %14.491
74 [I1, I2] = ind2sub(size(results_arr_pk),I);
75 optimal_freq = TMD_freq_range(I1)
76 optimal_freq_ratio_nom = optimal_freq/str_mid_freq
77 optimal_damp = TMD_damp_range(I2)
78 M
79
80
81 %% plotting
82
83 delete(bar)

```

```
84
85 figure(1)
86 subplot(1,3,1)
87 surf(TMD_damp_range,TMD_freq_range,results_arr_avg,'EdgeColor','none')
88 title('average')
89 xlabel('TMD damping ratio (%cr)')
90 ylabel('TMD natural frequency (Hz)')
91
92 subplot(1,3,2)
93 surf(TMD_damp_range,TMD_freq_range,results_arr_pk,'EdgeColor','none')
94 title('peak')
95 xlabel('TMD damping ratio (%cr)')
96 ylabel('TMD natural frequency (Hz)')
97
98
99 subplot(1,3,3)
100 surf(TMD_damp_range,TMD_freq_range,results_arr_rms,'EdgeColor','none')
101 title('RMS')
102 xlabel('TMD damping ratio (%cr)')
103 ylabel('TMD natural frequency (Hz)')
104
105 sgtitle(strcat("TMD design parameter response surfaces for
    ",num2str(percent_freq_variability*100),"% frequency
    uncertainty for ",num2str(mass_ratio*100),"% mass ratio") )
```
